

Investigating the effects of a summer storm on the North Sea stratification using a regional coupled ocean-atmosphere model

Alexandra Gronholz · Ulf Gräwe ·
André Paul · Michael Schulz

Received: date / Accepted: date

Abstract The influence of a summer storm event in 2007 on the North Sea and its effects on the ocean stratification are investigated using a regional coupled ocean (Regional Ocean Modeling System, ROMS)-atmosphere (Weather Research & Forecasting model, WRF) modeling system. An analysis of Potential Energy Anomaly (PEA, Φ) and its temporal development reveals that the loss of stratification due to the storm event is dominated by vertical mixing in almost the entire North Sea. For specific regions, however, a considerable contribution of depth-mean straining is observed. Vertical mixing is highly correlated with wind induced surface stresses. However, peak mixing values are only observed in combination with incoming flood currents. Depending on the phase between winds and tides, the loss of stratification differs strongly over the North Sea. To study the effects of interactive ocean-atmosphere exchange, a fully coupled simulation is compared with two uncoupled ones for the same vertical mixing parameters to identify the impact of spatial resolution as well as of SST feedback. While the resulting new mixed layer depth after the storm event in the uncoupled simulation can still be located in the euphotic zone, the coupled simulation is capable to mix the entire water column while the vertical mixing without SST feedback is strongly amplified. These differences

Alexandra Gronholz
MARUM - Center for Marine Environmental Sciences and Department of Geosciences, University of Bremen
Klagenfurter Strasse, 28359 Bremen, Germany
Tel.: +49 (0)421 218 65433
E-mail: agronholz@marum.de

Ulf Gräwe
Leibniz-Institute for Baltic Sea Research, Warnemuende, Germany
Institute of Meteorology and Climatology, Leibniz University Hannover, Hannover, Germany

Andre Paul and Michael Schulz
MARUM - Center for Marine Environmental Sciences and Department of Geosciences, University of Bremen, Germany

have notable implications for ecosystem modeling since it could determine the development of new phytoplankton blooms after the storm and for sediment modeling in terms of sediment mobilization. An investigation of restratification after the extreme event illustrates the persistent effect of this summer storm.

Keywords Potential Energy Anomaly Analysis · North Sea Modeling · Ocean Stratification · Vertical Mixing · Ocean-Atmosphere Coupling

1 Introduction

The North Sea is a shallow shelf sea in northwestern Europe with a mean depth of 80 m. It has ecological significance since it is European's main fishery, accounting for more than 5% of international commercial fish caught. A key factor for each marine ecosystem is the ocean stratification. The interface between a warmer, lighter upper ocean layer and a cooler, denser deeper layer inhibits the exchange of water masses and thus the exchange of nutrients, oxygen or even phytoplankton strongly. Such conditions can be found in the North Sea during summer time, when the ocean surface heats up and a clear stratification develops in wide areas of the North Sea. During autumn, the increased surface wind stresses, caused by higher storm activity, and the drop in air temperature lead to a weakening of the vertical stratification. This can finally result in an almost homogeneously mixed water column during winter time. However, some parts of the North Sea, which show a combination of shallower water depths and strong tidal mixing, usually stay fully mixed during the whole year (Simpson, 1971; Holt and James, 1999; Holt and Umlauf, 2008). Mathis et al (2013) show a deepening of the thermocline from 15 - 20 m in summer time when strong surface warming occurs to 30 - 40 m due to increased wind intensity during autumn. The interaction of the mixed layer depth and the amount of available nutrients in this layer is the key factor for phytoplankton growth.

The mentioned examples show the significance of ocean stratification and destratification on the system and lead to this study, providing a closer look at the physical processes behind.

The usual summer situation in the North Sea was notably changed in June 2007 (see Fig. 1, middle and right side). During the summer stratification period, a strong summer storm event called 'Uriah' crossed the North Sea (same Fig., left side). When this storm passed by, it created a sudden and clear footprint in the Sea Surface Temperature (SST) signal, producing an SST drop of about 4 degrees, as shown in satellite data. The storm disturbed the development of a warmer upper ocean layer so that the SST after the storm, from 28 June onwards, in particular in the central North Sea differs by about 3 K from values expected for July as given in climatology data. This happens although the SST prior to the storm exceeded the mean June situation as shown in climatology data by about 5 K in the central North Sea. Nevertheless, when comparing SST at the end of June with a climatological mean of June SST,

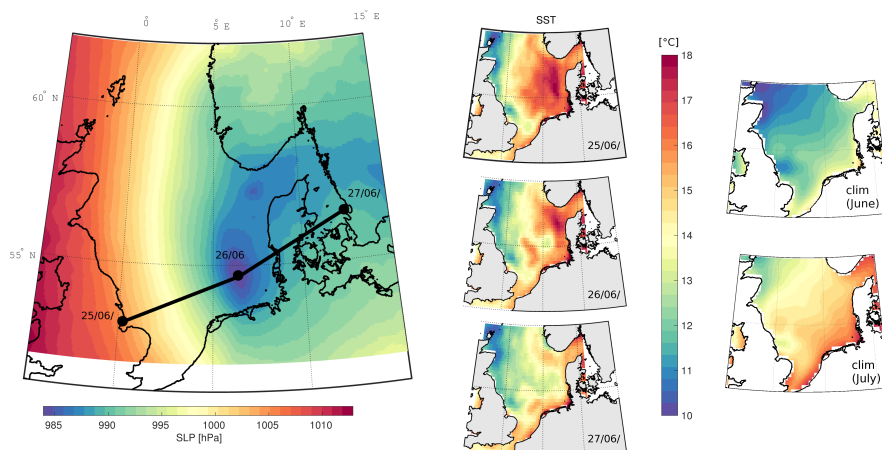


Fig. 1 Left: Atmospheric sea level pressure (SLP) during storm Uriah on 26 June 2007; black dots and line: storm track (line) and location of minimum surface pressure (dots) on 25, 26 and 27 June 2007 when crossing the North Sea (operational atmospheric model of the German service Deutscher Wetterdienst (DWD)); Middle: Sea surface temperatures on 25, 26 and 27 June as seen by satellite (Reynolds et al, 2007); Right: climatology data for June and July; for lat/lon information see left figure

it has to be considered that the storm crossed the North Sea at the end of June, while during that month a strong increase of SST is continuously forced, leading to a decrease of the SST mean. Analyzing the SST cooling structure, it is not obvious which physical processes lead to this temperature change, since SST data only show the ocean surface behavior.

From the mentioned observed SST changes, changes in the stratification have to be expected, but also other physical processes might be involved and interact. To investigate in detail which processes governed stratification and destratification during this storm event, an analysis of potential energy anomaly (PEA or Φ), as a measure for stratification, is conducted. To calculate the single Φ terms, which mainly depend on the vertical and horizontal structures of density and velocities, a 3-dimensional coupled ocean (ROMS)-atmosphere (WRF) system, based on the COAWST (Coupled Ocean-Atmosphere-Wave-Sediment transport) system (Warner et al, 2010) is set up for the North Sea region. Various previous studies and model simulations regarding general stratification processes in the North Sea as well as its oceanography exist. A general overview and inter-comparison of different existing uncoupled numerical ocean models covering the North Sea region can be found in Delhez et al (2004) or Lenhart and Pohlmann (2004), for instance. (De-) Stratification and mixing processes in the North Sea have been investigated and explained in the past in several studies but those studies were all based on uncoupled simulations and/or focusing on long-term processes (Holt and James, 1999, Pohlmann, 1996, Holt and Umlauf, 2008, Simpson and Hunter, 1974, Schrum et al, 2006, among others). A recent study by Mathis et al (2013) presents a success-

ful setup of an uncoupled modeling system which can be used for dynamical downscaling in the North Sea region and thus as a useful tool to investigate climate change scenarios on a regional scale, for instance. But again, all of those mentioned applied models are collectively uncoupled simulations. Groeger et al (2015) compare interactively and passively coupled simulations of the Baltic and North Sea. They found that interactive coupling brings additional advantages for the simulations since it considerably improves the simulated winter sea surface temperatures. They conclude that interactive coupling is mostly important in winter when strong winds occur. In summer under stratified situations with less winds, they state, interactive coupling is less important. However, their study focuses on general or typical conditions during the year. Thus, the impact under unusual conditions during extreme events like a strong summer storm under stratified conditions is still unclear.

Several previous studies which apply a coupled ocean-atmosphere system outside of the North Sea region (mainly for storm research focusing on the atmospheric component) highlight the non-negligible interaction of both components during a sudden event (for instance Sun et al, 2015, Perrie et al, 2004 or Pullen et al, 2007). Nevertheless, one arising question is, whether a coupled simulation in this region is capable to bring advantages and value compared to an uncoupled simulation. As shown in Fig. 1, a clear reduction of SST occurred during this unusual summer storm event. Thus a noticeable change of the SST can be expected during this particular short term event, which might have an influence on the system, in terms of wind velocity changes for instance. This is in contrast to winter storm events crossing an already well-mixed North Sea. This precondition makes them almost unable to influence SST which in turn prevents the atmosphere from experiencing a change in the oceanic feedback via SST.

In this study, three different setups will be compared to investigate the impacts of the ocean feedback in terms of SST exchange as well as higher spatial and temporal resolution of forcing data. This is done by a comparison of two uncoupled simulations with a coupled simulation. However, it should be noticed that the focus of this study is not intended to be on an in-depth comparison between coupled and uncoupled simulations but rather on the analysis of physical processes regarding the destratification process during a summer storm. A number of different physical processes could potentially act as drivers for the observed SST changes and thus for the loss of stratification, such as atmospheric cooling, advection, different straining mechanisms or vertical mixing. After an overview of model setups and the theory for the calculation of Φ and the Φ terms (Sec. 2), in Sec. 3 the results of this study are presented. These results firstly include an evaluation and secondly show the spatial and temporal development of Φ and the single Φ terms during the short-term extreme event. In Sec. 4 results are discussed and related to consequences for the North Sea system.

2 Methods and data

2.1 Observational data

CTD (Conductivity, Temperature, Depth) data are used to evaluate vertical and horizontal temperature and salinity structures. The measuring devices were mounted on a Scanfish (EIVA a/s, Denmark) and were taken in August 2007 in adjustable V-curved undulation path mode and in the depth range from 5 m to 60 m below the surface. Sampling transects are part of the monitoring program of the German Bundesamt für Seeschifffahrt und Hydrographie (BSH, Loewe et al (2013)) and take place every year (since 1998) in July/August.

For the evaluation of SST, the observational dataset of Reynolds et al (2007) is used, which is a combination of satellite observations at different wavelength, in-situ measurements and optimal-interpolation. This product is provided in a daily temporal and 0.25° spatial resolution.

Wind fields are evaluated with data from the operational atmospheric model of the German Deutsche Wetterdienst (DWD). These simulations have a spatial resolution of 7 km and a temporal resolution of 3 hours.

To evaluate the model behavior in time, two buoy datasets taken from the Centre for Environment, Fisheries and Aquaculture Science (CEFAS, Great Britain) are used. For the two stations Anasuria and Oysterground (for location see Fig. 2) hourly time series of near sea surface temperature are extracted from the database. For the physical analysis, beside the station Oysterground a further virtual station is selected. The station is placed in the region of largest stratification changes and referred to as HPC, standing for High Φ Change area, see Fig. 2.

For the evaluation of the sea surface height an hourly time series at the gauge Helgoland is used.

2.2 COAWST modeling system

In this study, the coupled ocean-atmosphere-wave-sediment transport (COAWST) (Warner et al, 2010) system Version 3.1 is applied. The COAWST system was developed to study coastal processes at regional scales and their interactions and is applicable, among others, to shelf environments (Warner et al, 2008) as given in the North Sea region. COAWST includes four different components: The atmosphere model WRF (Weather Research & Forecasting Model), the ocean model ROMS (Regional Ocean Modeling System), sediment transport capabilities of the Community Sediment Transport Model and the wave model SWAN (Simulating WAVes Nearshore (Booij et al, 1999)). The single components are able to communicate using the Model Coupling Toolkit (MCT, Jacob et al (2005) and Larson et al (2005)). In the COAWST system, data exchange of prognostic variable fields in user-defined individual time intervals is pro-

vided. In this study, a time interval of 10 minutes is chosen for a frequent data exchange during the investigated storm event. For simplicity the number of coupled components is limited to the atmosphere model WRF and the ocean model ROMS, as described in the following section. When applying WRF, it provides surface data as surface heat fluxes, surface stresses and all fields for the freshwater flux, such as atmospheric pressure, relative humidity, atmospheric surface temperature and precipitation, to ROMS. In the coupled setup, ROMS additionally hands over SST information to WRF.

2.2.1 Weather Research & Forecasting Model - WRF

The Weather Research and Forecasting (WRF) model (Skamarock et al, 2008) is an atmospheric non-hydrostatic simulation and numerical weather prediction system, developed by the National Center for Atmospheric Research (NCAR).

In this study, the '2m' resolution is taken for static terrestrial data (which include soil-type, land-use and other data). This corresponds to an approximately 4 km horizontal resolution of these terrestrial data used for the interpolation to the model grid. Boundary conditions are created from the 1 x 1 degree global NCEP Final Analyses (FNL) with 6-hourly resolution on 26 pressure levels (1000 - 10 hPa excluding surface). The WRF grid is created with a horizontal resolution of approximately 10 km and it includes 28 vertical layers. The time step is set to 60 seconds. The chosen WRF domain covering the North Sea is equivalent to the chosen ROMS domain (see Fig. 2). For the WRF-uncoupled simulation, required SST data are taken from the NCEP Real-Time SST archive. The applied physical options follow Berg et al (2013), who set up a WRF application for the European (42 km resolution) and German (7 km resolution) region. Applied physical options are: as cumulus parameterization the Kain-Fritsch scheme; the Noah land surface model; for the parameterization of microphysics the WRF Single-Moment 5-class scheme; to represent the planetary boundary layer the Yonsei University scheme; for the surface layer the MM5 surface layer scheme and to represent the longwave radiation the Rapid Radiative Transfer Model (RRTM) scheme.

2.2.2 Regional Ocean Modeling System - ROMS

The Regional Ocean Modeling System (ROMS) is used to simulate the ocean. ROMS is a free-surface, terrain-following coordinate oceanic model which uses the hydrostatic and Boussinesq approximations to solve the three-dimensional Reynolds-averaged Navier-Stokes equations on an Arakawa C grid (Shchepetkin and McWilliams, 2005, Haidvogel et al, 2008). In this study, the GLS scheme (Warner et al, 2005) is used and parameters are selected corresponding to the k - ϵ closure scheme.

The ROMS grid has a horizontal resolution of $1/6^\circ$ longitude and $1/10^\circ$ latitude (which corresponds to a resolution of about 10 km) and a vertical resolu-

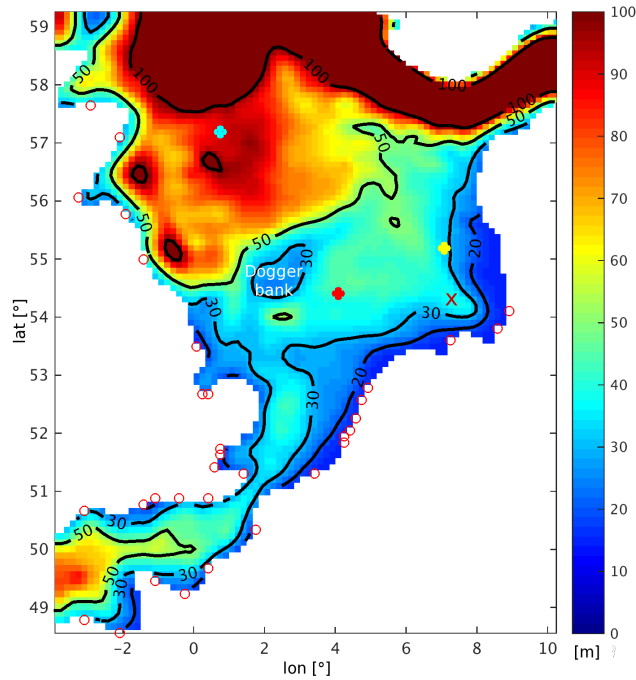


Fig. 2 ROMS domain with landmask and bathymetry data in m; for visualization purposes the colorscale is clipped at 100 m; stations Oysterground (red dot), Anasuria (light blue dot) and HPC area (yellow dot, see Sec. 3.4.1); Helgoland (red cross); river locations for freshwater input (red circles)

tion of 30 layers. The domain is equivalent to the applied WRF domain and is shown in Fig. 2. Bathymetry data are smoothed with a threshold r-factor value (which stands for the maximum slope of topography allowed in smoothing) of 0.25. This smoothing is applied to avoid a too strong influence by the pressure gradient error, which is known to arise in sigma-coordinate models in areas with steep bathymetry (Haney, 1991).

Lateral boundary conditions of temperature, salinity and sea surface elevations are extracted from the daily output of the HYbrid Coordinate Ocean Model (HYCOM), which provides a global 1/12 degree reanalysis (Chassignet et al, 2007). Tides are prescribed at the open boundaries by superimposing on HYCOM data using the OSU Tidal Inversion Software (OTIS) (Egbert et al, 1994; Egbert and Erofeeva, 2002) after Penven et al (2007). Surface forcing for ROMS is either provided by WRF (in the coupled and in the WRF-uncoupled simulation) or by ERA-Interim data (in the following called ERA) using bulk formulas. which offer 3-hourly surface fields and a spatial resolution of approximately 80 km (T255). For further information see ECMWF (August 2016).

To produce an appropriate salinity structure, 33 river source points are included. Each of those point sources represents one river, except for the Rhine, which is split into 5 source points to avoid numerical instabilities due to the

very strong Rhine inflow and the resulting strong salinity gradient. Transient river input data with daily resolution are taken for that time period from the river database of the Centre for Environmental Prediction (CEFAS, Great Britain). An overview of all river mouth locations is also shown in Fig. 2.

2.3 Potential energy anomaly

To express the strength of stratification in the ocean, the potential energy anomaly (PEA, Φ) is used. Φ can be understood as energy required to completely mix the water column and is given in J/m^3 . It has been derived by Simpson et al (1981) and Simpson and Bowers (1981) as the depth integral over the deviation of potential density from the mean potential density of the water column and thus from mixed conditions, as

$$\Phi = \frac{1}{D} \int_{-H}^{\eta} gz(\bar{\rho} - \rho) dz \quad (1)$$

with the vertical coordinate z from $z = -H$ at the bottom to $z = \eta$ at the sea surface, the gravitational acceleration g , the water depth D given as $D = \eta + H$, ρ represents the potential density and $\bar{\rho}$ its vertical mean

$$\bar{\rho} = \frac{1}{D} \int_{-H}^{\eta} \rho dz. \quad (2)$$

If Φ values are zero, the local potential density and the mean density of the water column are identically which represents a homogeneously mixed water column. In contrast, high Φ values occur in a situation of strong stratification, indicating a stable stratification with positive values and an unstable stratification with negative values. Burchard and Hofmeister (2008) describe an analytical way to calculate a dynamic equation for Φ based on the dynamic equations of potential temperature and salinity, the continuity equation and an equation of state for the potential density. Using this formulation it is possible to specify several terms representing different physical processes responsible for the change in Φ over time as follows:

$$\begin{aligned} \partial_t \Phi = & \underbrace{-\nabla_h(\bar{\mathbf{u}}\Phi)}_A + \underbrace{\frac{g}{D}\nabla_h\bar{\rho} \int_{-H}^{\eta} z\bar{\mathbf{u}} dz}_B - \underbrace{\frac{g}{D} \int_{-H}^{\eta} (\eta - \frac{D}{2} - z)\bar{\mathbf{u}} \cdot \nabla_h\bar{\rho} dz}_C \\ & - \underbrace{\frac{g}{D} \int_{-H}^{\eta} (\eta - \frac{D}{2} - z)\bar{w}\partial_z\bar{\rho} dz}_D + \underbrace{\frac{\rho_0}{D} \int_{-H}^{\eta} P_b dz}_E - \underbrace{\frac{\rho_0}{2}(P_b^s + P_b^b)}_F \\ & + \underbrace{\frac{g}{D} \int_{-H}^{\eta} (\eta - \frac{D}{2} - z)Q dz}_G + \underbrace{\frac{g}{D} \int_{-H}^{\eta} (\eta - \frac{D}{2} - z)\nabla_h(K_h\nabla_h\rho) dz}_H \quad (3) \end{aligned}$$

using the horizontal velocity vector \mathbf{u} , the depth-averaged horizontal velocity vector $\bar{\mathbf{u}}$

$$\bar{\mathbf{u}} = \frac{1}{D} \int_{-H}^{\eta} \mathbf{u} dz \quad (4)$$

the deviation from the depth-averaged horizontal velocity vector as

$$\tilde{\mathbf{u}} = \mathbf{u} - \bar{\mathbf{u}} \quad (5)$$

the horizontal gradient operator ∇_h , the vertical and horizontal eddy diffusivity K_v and K_h , the vertical buoyancy flux P_b

$$P_b = \frac{g}{\rho_0} K_v \partial_z \rho \quad (6)$$

with the surface buoyancy flux P_b^s and the bottom buoyancy flux P_b^b , the source term Q for density

$$Q = -\frac{\rho\alpha}{\rho_0 C_p} \partial_z I + K_v \partial_z \theta \partial_z (\rho\alpha) - K_v \partial_z S \partial_z (\rho\beta) \\ + K_h \nabla_h \theta \cdot \nabla_h (\rho\alpha) - K_h \nabla_h S \cdot \nabla_h (\rho\beta) \quad (7)$$

with α as thermal expansion coefficient, β as haline contraction coefficient, I as shortwave radiation and C_p as heat capacity. For further information and the detailed derivation of Eq. 3 see Burchard and Hofmeister (2008).

Tab. 1 gives an overview of the single Φ terms, their physical meaning as well as typical processes driving these terms and corresponding typical time scales.

Term A and D represent horizontal and vertical advection respectively. Term B, the depth-mean straining, identifies changes in Φ due to a horizontal gradient in depth-mean density and a vertically sheared flow. Term C, the non-mean straining, may create a change in Φ even if the mean density is equally distributed in the horizontal, but a vertical density gradient exists. The vertical mixing is mainly driven by intense surface stresses but also tides have an influence on term E. Term F represents the heat fluxes and thus is strongly influenced by solar radiation. Inner sources and sinks (term G) may occur if denser or lighter water is created somewhere in the water column supporting either stratification or destratification. Term H corresponds to horizontal mixing.

In this study, Φ values and the single Φ terms are calculated for the North Sea as described above. Furthermore, the most important terms are identified for the entire North Sea. This is done a) prior to the storm event to represent standard conditions and b) during the event for a comparison. Regarding the standard conditions, values are calculated by integrating the behavior of all terms (right side of Eq. 3) between 21 June and 25 June 2007 from hourly model output and by defining the most influencing term during this period. An integration over that time interval was taken to filter out smaller scale variability of the single terms. Regarding the storm period, the main terms responsible for Φ change are calculated between 26 and 28 June, again to filter out smaller scale processes but also to consider the travel time of the storm event across the entire North Sea.

Table 1 Overview of single Φ terms their physical meaning and typical main forcing processes and typical time scales (TS)

Term	Physical meaning	Typical main forcing	TS [hours]
A	Φ advection	currents (residual, tides)	12
B	depth-mean straining	currents (tides)	12
C	non-mean straining	currents (tides)	12
D	vertical advection	currents (residual, tides)	12
E	vertical mixing	surface stresses	n/a
F	surface and bottom buoyancy fluxes	solar radiation	24
G	inner sinks and sources	solar radiation	24
H	divergence of horizontal transport	currents (horizontal shear)	n/a

3 Results

3.1 Summer storm Uriah

The seasonally unusual low pressure system Uriah developed first on 23 June 2007 over the North Atlantic. It hit the shelf region on the 24 June, moved over the Irish Sea and reached the region of the English Channel on the morning of 25 June with a central pressure of less than 1000 hPa. It crossed the North Sea between 25 and 27 June from south-west to north-east. The pathway of storm Uriah when it crossed the North Sea is shown in Fig. 1. A clear footprint of the storm can be seen in the SST. Uriah produced a surface temperature drop of about 4 K in the central North Sea and the surface pressure fell further by 30 hPa. At this time, the 2 m air temperature showed lowest values with a total cooling of about 5 K during this event. Highest wind speeds developed over the central North Sea with more than 20 m/s. When the storm hit the coast of Denmark (27 June) it already lost some of its intensity and the wind speed were reduced by more than 5 m/s.

3.2 Evaluation of wind fields

The main influence of the atmosphere in this summer storm study is expected to result from the surface wind forcing. To evaluate the model results at the air-sea interface, wind velocity data from the operational atmospheric model of the DWD are used for a comparison (Fig. 3). The comparison indicates a good agreement in both, wind intensity and general patterns. Likewise, additional comparisons with further datasets (for instance using observational data from IFREMER CERSAT Global Blended Mean Wind Fields, not shown) show a similar agreement. The passing storm event can clearly be identified in both

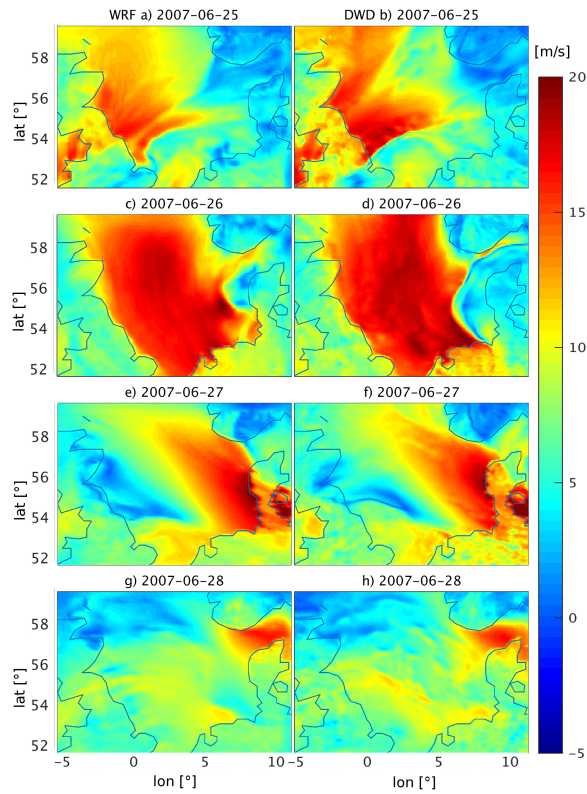


Fig. 3 Comparison between WRF and DWD wind speeds at 10 m height ($|U_{10m}|$ in m/s) for different snapshots between the 25 and 28 June. The left column shows the WRF results, the right column presents the data from the operational German weather forecast model (DWD).

datasets.

3.3 ROMS evaluation

3.3.1 Time series of Sea surface height (SSH)

As a measure to validate the model simulation, ROMS sea surface heights (SSH) are compared to available SSH data at Helgoland (see Fig. 2 for the location of Helgoland and Fig. 4 for the SSH comparison). This location was chosen since it offers continuous data during the relevant year 2007. The general temporal developments of both time series show similar behavior, indicating storm events to occur mainly at the same time. Datasets of residual SSH agree with a correlation coefficient of about 0.8 and a root mean square error (RMSE) of less than 0.2 m. The complete SSH data, including tides, agree

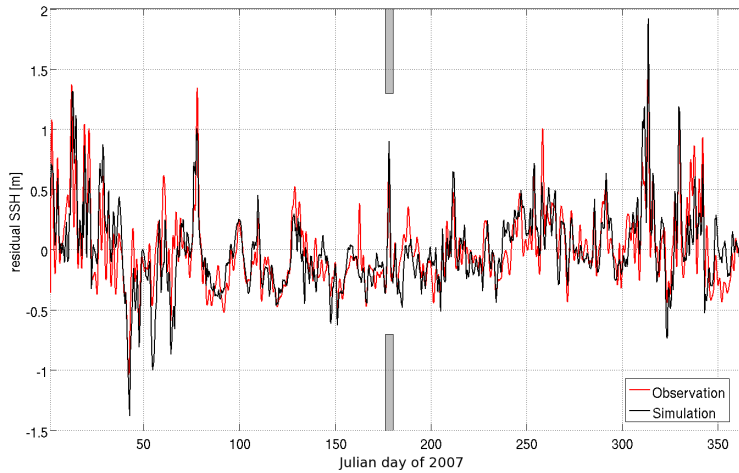


Fig. 4 Comparison of residual sea surface height (SSH) at station Helgoland in coupled simulation (black) and observations (red) for 2007; indicated in gray: storm period 25 - 29 June

with an RMSE of 0.5 m and with a correlation coefficient of 0.79. The peak elevation of 0.9 m is well captured by the model with 0.78 m.

3.3.2 Sea surface temperature (SST)

In a second step, SST satellite data (see Sec. 2.1) are used to validate ROMS results at the ocean surface for coupled and uncoupled simulations. The left row of Fig. 5 shows the temporal development of the SST pattern during the summer storm event between 24 and 28 June 2007 as seen by the satellite. The observations show a clear signal in terms of a storm footprint on 26 and 27 June. The SST decreases by about 4 K in the central North Sea where a considerable stratification had been present before (see Fig. 6) with very warm ocean surface layers. All simulations are capable to produce the footprint of storm Uriah on 26 and 27 June. With about 4 K in the central North Sea, the relative SST drop has a comparable magnitude in the coupled and the ERA-uncoupled simulation. The WRF-uncoupled simulation shows already prior to the storm event too cold SST by about 1-2 K. Therefore the relative drop in SST due to the storm is about 1 K less. The ERA-uncoupled simulation yields in general an overestimation of the SST in the central North Sea by 1 K. In the Norwegian Trench, all simulations differ from observations by partially higher SST values which is not the case during winter time.

3.3.3 Scanfish data

A comparison of coupled ROMS results and observations is shown for 55° (7 Aug 2007), 56° (9 Aug) and 57° (10 Aug) (Fig. 6). Temperature ranges as well

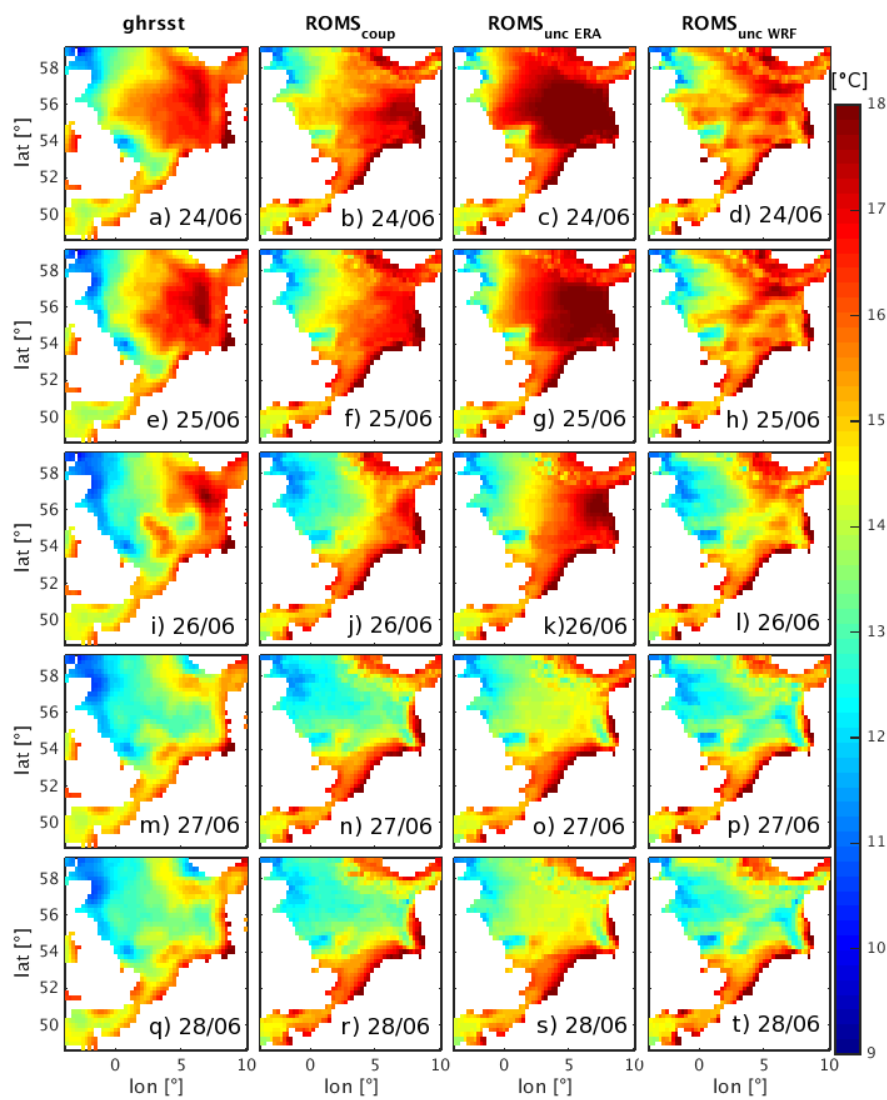


Fig. 5 Comparison of GHRST data (left) with ROMS SST data in coupled (left middle), ERA-uncoupled (right middle) and WRF-uncoupled (right) simulation

as the basic structures are represented by the model simulations. Comparing the sections at 55° , both cold water reservoirs, separated by the Dogger Bank, are visible. The eastern “reservoir” tends to be warmer and smaller in extent compared to the observations. This could arise from the applied horizontal resolution of approximately 10 km and thus a blurring of the signal. In some areas, temperatures near the surface tend to be warmer than observations by about 1 K. Sections 56° and 57° have similar properties. The surface mixed

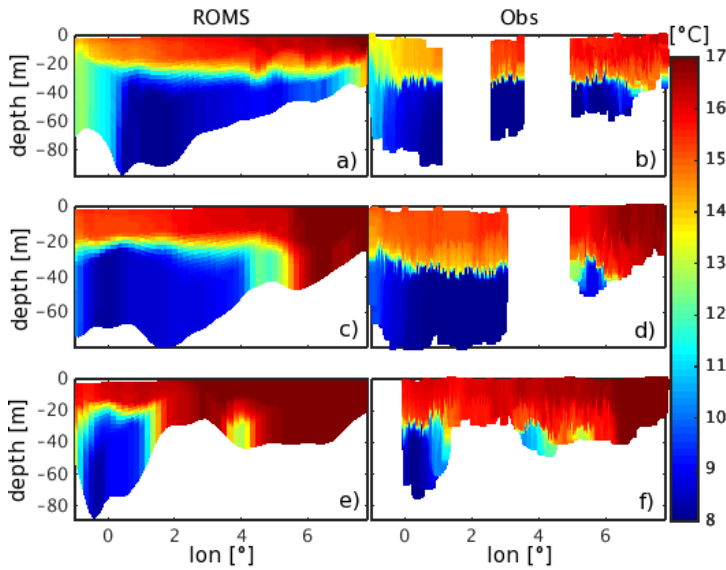


Fig. 6 Temperature in °C; comparison of coupled ROMS results (left) and Scanfish data (right) at 57° on 10 August (a & b), 56° on 9 August (c & d) and 55° on 7 August (e & f)

layer (SML) tends to be thinner by about 5 m and near surface temperatures are warmer by about 0.5 K - 1 K than observations. The sharpness of the thermocline as given in observations cannot be represented by the use of the applied vertical resolution (30 layers). Nevertheless, overall the ROMS results shown in the sections are in an adequate agreement with observations for the purpose of this summer storm study.

The evaluation of the salinity structures (Fig. 7) indicates that the spatial pattern and salinity ranges are represented to a reasonable degree in the simulations. At 55° latitude model results capture the low salinity area west of 1° longitude for instance and this section as well as the section at 56° latitude show the low salinity structures to the east of 6° longitude. The section at 57° latitude (a & b) indicates the low-salinity outflow of the Baltic Sea.

3.3.4 Time series of Temperature

To compare the general temporal development of sea surface temperatures as well as the difference between the coupled and the uncoupled simulations, two fixed observational datasets are used (Fig. 8). One station is located in the north-western North Sea (called Anasuria), the other one in the central North Sea (called Oysterground).

Both stations clearly indicate an overestimation of surface temperatures in the ERA-uncoupled run during summer time, starting approximately at day 150 (which corresponds to the beginning of June) and in particular during the Uriah summer storm event. This simulation overestimates the SST during the

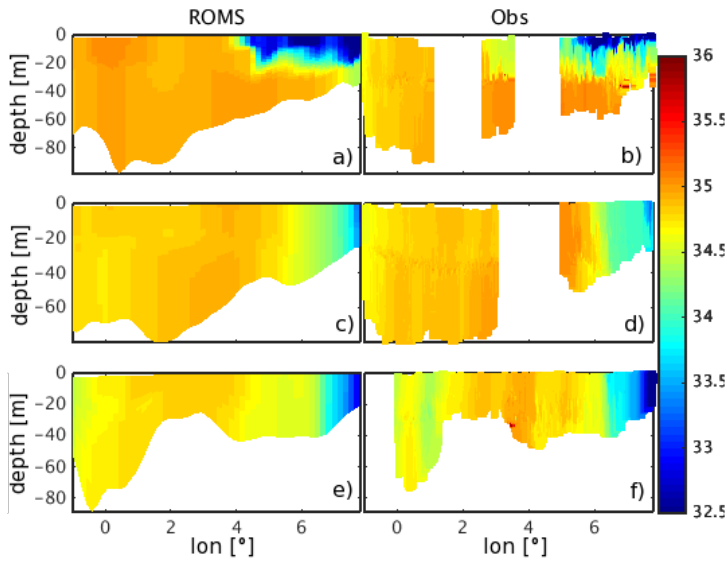


Fig. 7 Salinity; comparison of coupled ROMS results (left) and SCANFISH data (right) at 57° on 10 August (a & b), 56° on 9 August (c & d) and 55° on 7 August (e & f)

storm event compared to observations by about 1.3 K and prior to the storm even by approximately 3.2 K. Furthermore, in the ERA-uncoupled simulation, the storm event is not capable to produce the final minimum SST as given in the observational dataset. Instead the SST is approximately 1.1 K too warm directly at the end of the storm. Results of the WRF-uncoupled simulation show opposite behavior by underestimating the SST prior to the storm event by about 1 K at Oysterground. At Anasuria, until day 220 the WRF-uncoupled simulation agrees with the coupled simulation while both match observations. Nevertheless, this agreement is limited to the north-western North Sea where Anasuria is located as shown in Fig. 5. At both stations the WRF-uncoupled simulation overestimates the SST strongest by about 1 to 2 K from day 220 onwards, although all simulations tend to overestimate SST here by at about 0.5 to 1 K.

The results of the coupled simulation range between both uncoupled simulations and follow the observations more closely during the investigated event, in particular in the central North Sea. Maximum observational SST values are reproduced in the coupled simulation and the final minimum temperature at the end of the event is, with a difference of about 0.3 K, closer to the observations as in red the ERA-uncoupled simulation but comparable to the WRF-uncoupled simulation. Prior to the storm at Anasuria both, the coupled and the WRF-uncoupled simulations agree better with the observations as the ERA-uncoupled one does (the ERA-uncoupled simulation produces here again too high SST values), although all simulations are too warm by about 0.2 K. In summary, since the focus of this study is on the Uriah summer storm event and its effects on the central and eastern North Sea, the coupled simulation is

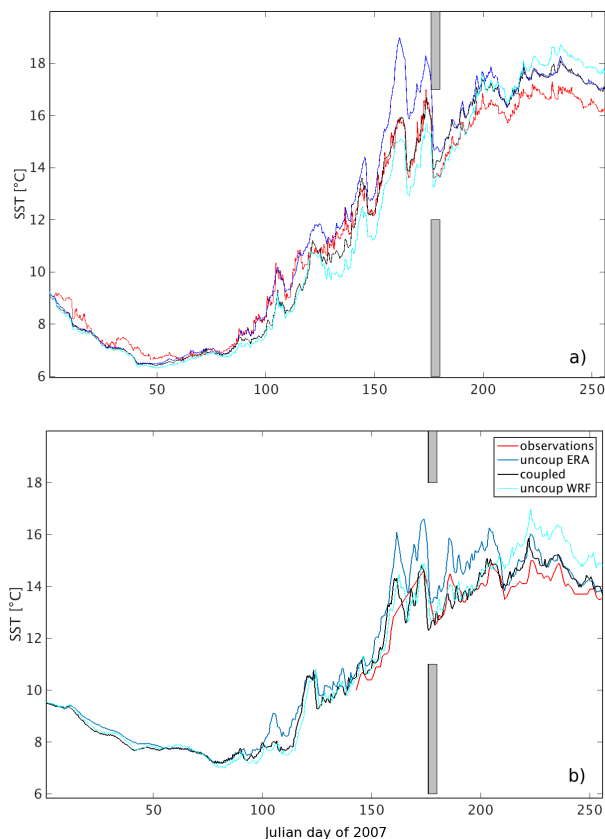


Fig. 8 Sea surface temperature comparison at stations Oysterground (a) and Anasuria (b); observations (red), ERA-uncoupled (blue), WRF-uncoupled (cyan) and coupled (black) simulations; indicated in gray: storm period 25 - 29 June

found to agree best with the observations, which is in agreement with previous studies (e.g. Schrum et al, 2003).

3.4 Potential energy anomaly

3.4.1 Spatial structure

When investigating the spatial structure of Φ , the general dependency of its calculation on water depths has to be kept in mind. As Φ can be interpreted as the energy needed to mix the entire water column, its values increase with increasing depth and may not be directly compared with mixed layer depths. Nevertheless, the bathymetry of the shallow central and eastern North Sea, which is the area of main interest in this study, is relatively constant and varies only by about 15 m (Fig. 2). Furthermore, the well-mixed areas are in agree-

ment with previous studies (e.g. Mathis et al, 2013) describing thermocline depths and mixed regions in the North Sea.

The general spatial structure of Φ for common summer conditions (Fig. 9a) reveals that Φ values in the southern North Sea approach zero. This is caused by the combination of strong tidal mixing and shallow water depth allowing the occurrence of an almost homogeneously mixed water column even during summer time. The location of this tidal front is further influenced by the interaction of tides, winds and buoyancy input (Simpson, 1971; Simpson et al, 1981). This was also illustrated by Holt and James (1999), who investigated the development and breakdown of the tidal mixing front during the year. This front separates well-mixed waters in the southern and eastern North Sea from stratified waters in the deeper central and northern regions. This front can be found in a similar shape in Fig. 9a at the Atlantic entrance to the English Channel.

In the central North Sea Φ values increase except for the region around the shallower Dogger Bank (for location see Fig. 2) which is known as a low-stratification tongue in the middle of the North Sea, marked by the $50 J/m^3$ contour line (black). The water column in this area is well mixed during the entire year, caused by the low water depth, which results in Φ values reaching zero. The study of van Leeuwen et al (2015) separates the North Sea stratification into several stratification types: i) permanently stratified, ii) seasonally stratified, iii) intermittently stratified, iv) permanently mixed and v) regions of freshwater influence. The Dogger Bank as well as the southern and very eastern North Sea areas are classified in their study as either permanently mixed or intermittently stratified (defined as showing less than 40 stratified days per year). This agrees very well with the mixed areas in this present study, indicated by low Φ values (Fig. 9a). In the north-western North Sea, where water depths increase, Φ reaches values of about $100 J/m^3$. Two high Φ areas can be found near the north England and south Scotland coastline, resulting from a very deep bathymetry in those regions. A similar behavior can be found in the Norwegian Trench, where Φ values are high due to high water depths. As Φ is a measure of energy needed to fully mix the water column, its values increase with increasing water depth; more energy is needed to mix the entire water column in such a case. In the study of van Leeuwen et al (2015), this area is classified as permanently stratified.

Prior to the event under standard conditions, a clear separation of the main Φ terms, that influence the stratification, can be found (Fig. 10). While the southern North Sea is mainly affected by vertical mixing (term E, rose), Φ changes in the central North Sea are mainly caused by surface fluxes (term F, red). In the north-western part of the North Sea, Φ changes are dominated by vertical advection (term D, green) and in the eastern North Sea by depth-mean straining (term B, dark blue). In addition, the central North Sea is also partially influenced by horizontal advection (term A, light blue).

During the storm event the situation changes considerably (see Fig. 10b). Changes of Φ in the southern, the central and the eastern North Sea, are now mainly caused by vertical mixing (term E, rose). Only smaller parts in the

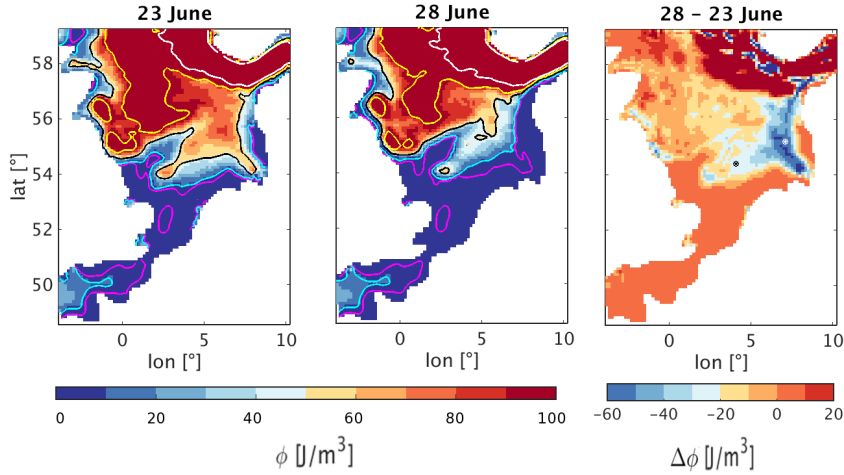


Fig. 9 Φ development; a) pre-storm (23 June), b) post-storm (28 June) and c) difference between 23 and 28 June ($\Delta\Phi$ given as 28 - 23 June); contour lines: 5=magenta, 10=cyan, 50=black, 100=yellow, 200=white; In c): analyzed stations Oysterground (black dot) and HPC (white dot). Please note the nonlinear colorscaling in a) and b) to emphasize details; results from coupled simulation

northern as well as in the western North Sea are influenced by either horizontal (term A, light blue) or vertical (term C, green) advection processes. Surface fluxes (term F, red) in the central North Sea cannot be identified as the main driver of Φ changes during the storm event anywhere in the central North Sea because they are completely masked by other processes (see also Fig. 11).

3.4.2 Time series

A comparison between stations Oysterground and HPC (black and white dots in Fig. 9c, respectively) for different parameters is shown in Fig. 11 and Fig. 12. At both locations a clear loss of stratification can be seen (in the HPC area about -50 Jm^{-3} , at Oysterground about -23 Jm^{-3}). At Oysterground this degeneration starts already slightly earlier around hour 130 compared to the HPC area where it starts around hour 150, which is due to the time the storm needs to cross the North Sea.

Prior to the storm, Φ values in the HPC area were higher compared to Oysterground, due to warmer surface layers for instance. For a thorough comparison of Φ and $\delta_t\Phi$ values at different locations, the influence of water depth has to be considered. Oysterground is located in an area of about 41 m depth, while the HPC area is about 32 m deep. These differences in the bathymetry are small (less than 9 m), which is generally the situation in the investigated shallow and flat central North Sea (see Fig. 2). It turns out that for the same water column conditions but a water depth artificially reduced by 9 m, the $\delta_t\Phi$

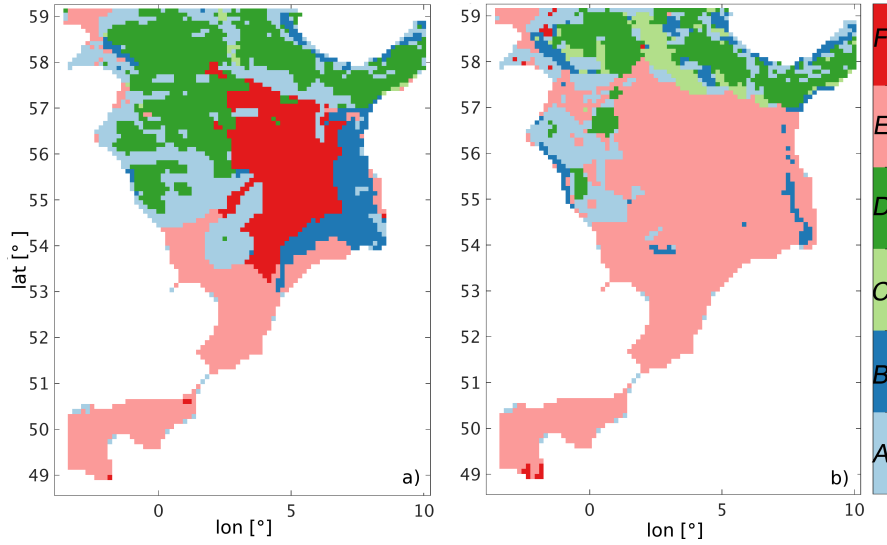


Fig. 10 Major terms (compare Eq. 3) changing Φ a) prior to the storm event between 21 June and 25 June 2007 (hours 1 to 100 in following time series figures), standard conditions and b) during the storm event around 26 and 27 June (hours 120 to 150 in following time series figures); results from coupled simulation

values differ by about $2.2 J/m^3$. This corresponds to less than 10% of the $\delta_t\Phi$ values at Oysterground. In conclusion, there is an influence of the water depths in the central North Sea, but it cannot be the main factor driving the strong differences in $\delta_t\Phi$ during the storm event, neither between Oysterground and HPC ($\delta_t\Phi$ difference is approximately $30 J/m^3$) nor in general in the central North Sea ($\delta_t\Phi$ difference maximum of about $60 J/m^3$).

The thermocline was lowered by the storm almost down to the bottom (to 32 m depth) whereas the thermocline at Oysterground was only lowered to approximately 25 m depths after the storm.

In a perfect case, the left side of Eq. 3 ($\delta_t\Phi$) and its right side ($\sum(A-H)$) exactly match. Also in this study, both sides of the equation match to a high degree (Fig. 11b and 12b). Although the comparison indicates some deviations between the red and the black curve, the overall behavior of both curves at both locations is in good agreement. This increases the confidence in the calculations based on Eq. 3. The deviation (black bars in both panels d) between the red and black curves (both panels b) is included as an indication of the significance of the individual terms in relation to a potential inaccuracy.

Term G (inner sinks and sources) does not become negligible as for instance found by Purkiani et al (2015). Terms A - D show an approximately 12-hourly oscillation whereas terms F and G show an 24-hourly oscillation. In standard conditions, prior to the storm, an analysis reveals that the terms A and C (horizontal advection and non-mean straining) and also terms B and D (depth-mean straining and vertical advection) have simultaneously either a

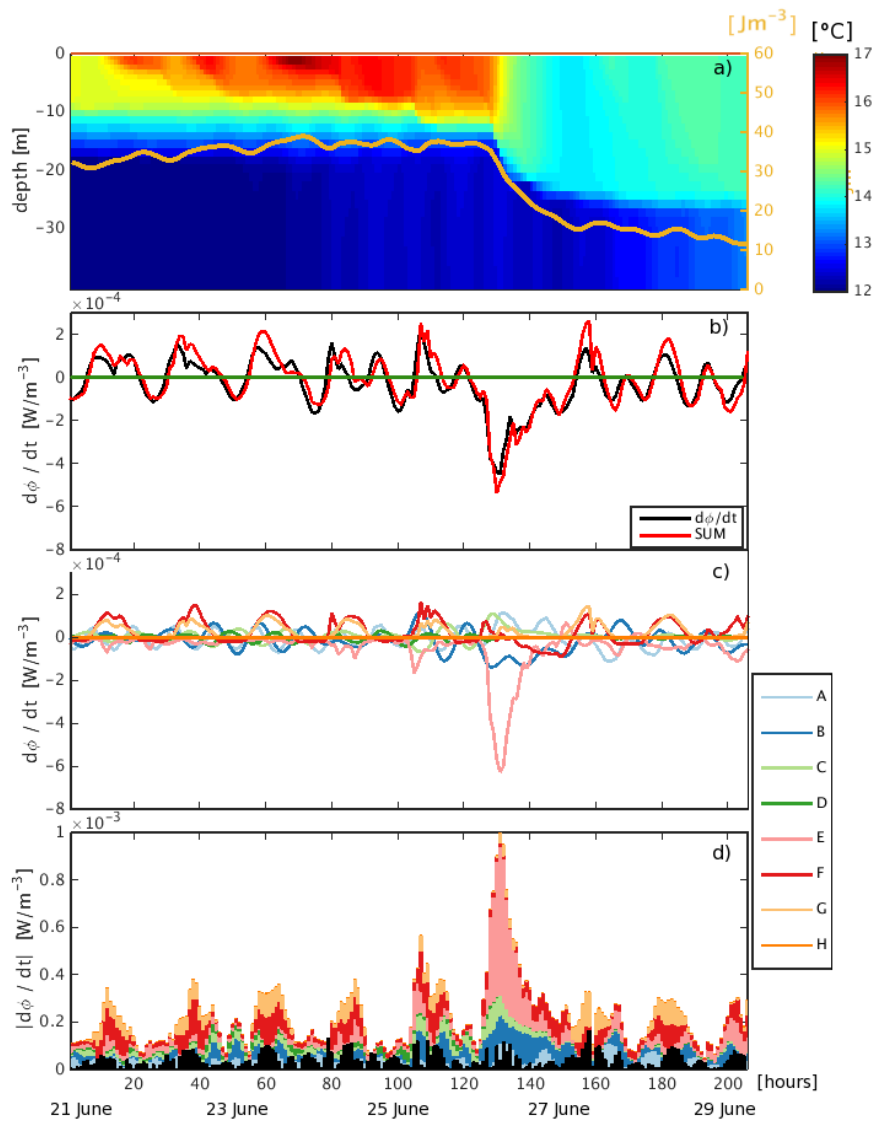


Fig. 11 Time series in hours between 21 and 29 June 2007 in coupled simulation at Oyster-ground, see Fig. 9c, black mark; a) temperature (colors) and total PEA Φ (brown line); b) $d\Phi/dt$ and sum of terms A-H, c) all terms, d) ratio of single terms. The black bars indicate the numerical error estimated as the difference between the red and black line from b)

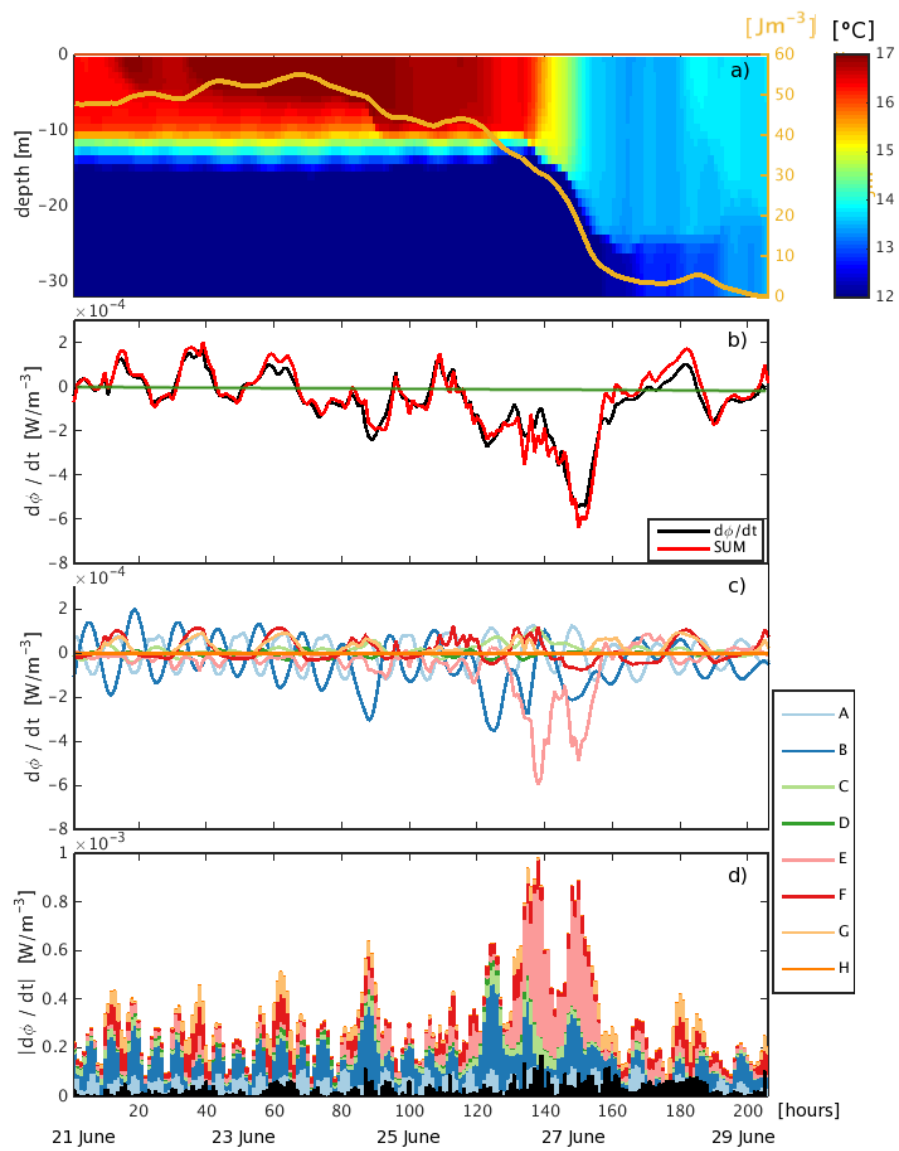


Fig. 12 Time series in hours between 21 and 29 June 2007 in coupled simulation for station HPC, see Fig. 9c, white mark; a) temperature (colors) and total PEA Φ (brown line); b) $d\Phi/dt$ and sum of terms A-H, c) all terms, d) ratio of single terms. The black bars indicate the numerical error estimated as the difference between the red and black line from b)

positive (enhancing stratification) or negative (destratifying) tendency. Terms A and C counteract terms B and D. This is a result of the strong dependency of these four terms on the tidal currents, which will be explained in the discussion section in more detail.

Regarding the 24-hourly oscillations it can be seen that terms F and G (surface fluxes and inner sources) influence stratification or destratification simultaneously in the same direction, when positive. Term G always either stays positive and thus either leads to stratification or has no impact (when becoming zero) for periods when term F becomes negative for instance. The behavior of these two terms is driven by the solar cycle, as explained closer in the discussion section.

At both locations, the vertical mixing (term E) has the main impact on the destratification. While the time series of vertical mixing at Oysterground only shows one peak, in the coupled simulation in the HPC area two distinct vertical mixing events occur. The time lag between these two mixing events is 12 hours, which can be associated with a semidiurnal tidal cycle. The ERA-uncoupled simulation however in the HPC area shows again only one vertical mixing signal while the WRF-uncoupled simulation shows the second signal, which in contrast leads to restratification (Fig. 13c).

The horizontal advection (Fig. 13a) shows notable differences during the storm event between the simulations: While the ERA-uncoupled simulation does not show an intensified stabilization of stratification but even a destabilization ($\delta_t\Phi$ almost zero), the WRF-uncoupled simulation shows a strong stabilization ($\delta_t\Phi$ of about $2 \times 10^{-4} \text{ W/m}^{-3}$), and the coupled simulation shows values in between ($\delta_t\Phi$ of about $1.2 \times 10^{-4} \text{ W/m}^{-3}$). The influence of vertical advection completely vanishes after the storm event in the WRF-uncoupled simulation. Regarding the effects on depth-mean straining (Fig. 13b), the ERA-uncoupled simulation tends to still show a stabilizing effect, the WRF-uncoupled simulation leads to a destabilization during the entire event and the coupled simulation ranges in between.

3.5 Thermocline deepening

The storm event also had a notable influence on the thermocline (Fig. 14). Following Mathis et al (2013), the thermocline depth is calculated by defining the maximum vertical temperature gradient, given by the change in temperature over a certain vertical distance, but only for values larger than 0.1 K/m . If the gradient is smaller than this threshold, the water column is taken as completely mixed (white areas in Fig. 14). Areas near the eastern coastline show a shallower thermocline prior to the storm of up to 15 m compared to the central North Sea with about 20 m and the western North Sea with a thermocline depth of about up to 35 m. After the storm, the thermocline in the eastern North Sea is deepened by up to 30 m and an enlargement of the completely mixed areas can be seen (see the change in white areas from Fig. 14a to Fig. 14b). This enlargement and the net thermocline deepening (Fig.

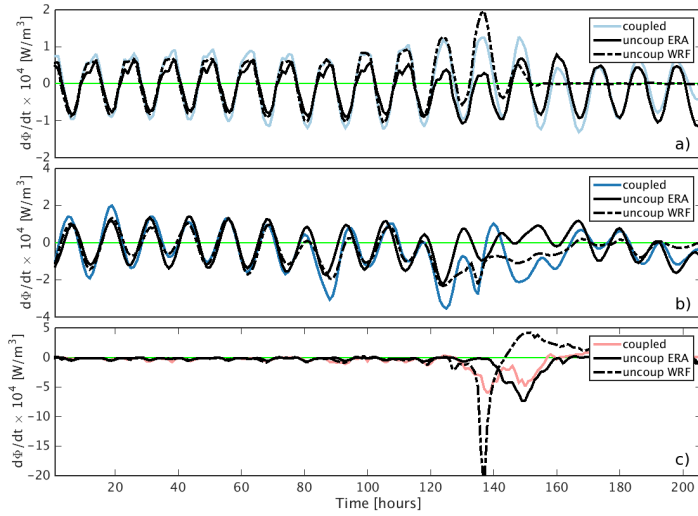


Fig. 13 Comparison of coupled and both uncoupled simulations at station HPC, see Fig. 9c white mark; a) Term A (horizontal advection), b) Term B (depth-mean-straining), c) Term E (vertical mixing); zero line in green

14c) reflect a stronger deepening of the thermocline in the eastern part of the North Sea (about 15 m or even entirely mixed) compared to the central part (about 5 m). This is in good agreement with the results of the areas of high destratification in the Φ analysis (Fig. 9c) and resulting differences for the locations Oysterground and HPC area. While at Oysterground a deepening of the thermocline of 8.9 m occurs, it deepens at HPC area from about 13 m completely up to the bottom at 32 m which results in a change of about 19 m. The mean thermocline deepening for the entire North Sea due to the storm event is about 6 m. Prior to the storm a stronger gradient of about 0.5 K/m can be found in the eastern North Sea while the storm event creates a gradient of this magnitude by the sudden change in the upper water column in almost the entire North Sea.

4 Discussion

4.1 Model evaluation

The comparison with Scanfish temperature data shows a good agreement regarding the temperature structures as well as temperature ranges. Nevertheless, temperatures near the surface tend to be warmer than observations by about $0.5 \text{ K} - 1 \text{ K}$. This is caused by the comparatively thinner surface mixed layer (SML) of the model results partially of about 5 m. Due to the shallower thermocline, the temperature in the surface mixed layer needs to be higher, assuming identical surface heat fluxes and thus a constant heat storage. A

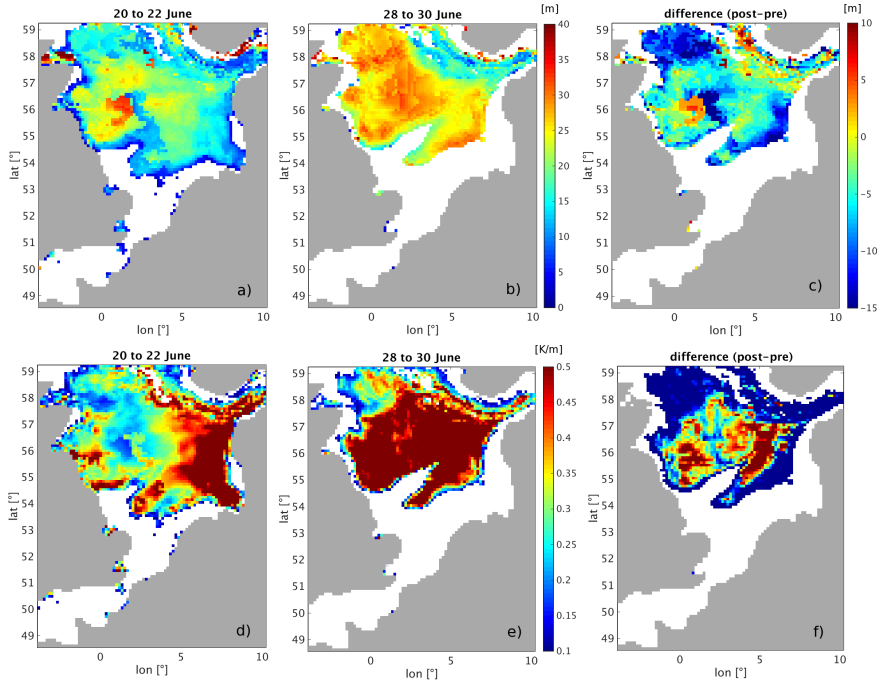


Fig. 14 Comparison of thermocline depth (a-c) and intensity (d-f) prior to the storm (a and d), afterwards (b and e) and the differences (post- minus pre-storm, c and f); results from coupled simulation

possible solution to deepen the thermocline could be a modification of the turbulence scheme to improve the simulation of internal waves, Langmuir circulation or injection of turbulent kinetic energy due to breaking waves, as discussed by Gräwe et al (2015). Focusing on the SST station data comparison, a similar effect can be seen: During the warming period after the storm event the coupled as well as the ERA-uncoupled simulation overestimates the SST almost uniformly by about 1 K. This is again caused by the too thin simulated SML. The WRF-uncoupled simulation in contrast underestimates the SST. This is a result of the much stronger surface stresses when not applying the SST feedback to the atmosphere, as discussed in the following sections. In the colder north-eastern North Sea (Fig. 7), where generally a deeper thermocline of about 25 m exists, a stronger mixing has relatively less impact, which can be seen at station Anasuria, for instance.

The observed differences in the low salinity tongue originating from Baltic Sea outflow (the tongue is more mixed in the Scanfish observations compared to the simulation which shows a rather sharp transition from about 32.5 to 35) could either be an artifact resulting from data gaps around 4° longitude or could be driven by mesoscale activities in this area due to eddies coming off the coast.

The comparison of SST between model results and satellite data show in general an appropriate agreement regarding the structure as well as the order of magnitude, in particular in the coupled application. While the ERA-uncoupled simulation overestimated the observations due to the lower spatial resolution of the forcing data, the WRF-uncoupled simulation underestimates the observations, in particular before the storm event. Afterwards the entire North Sea is almost completely mixed and thus increased mixing cannot have any further effect on the SST. In the Norwegian Trench differences can be observed in all simulations. The SST behavior in the Norwegian Trench has to be analyzed carefully. In this deep region ROMS sigma coordinates get strongly stretched, resulting in thicker surface layers, compared to shallower areas. Those stretched layers are not directly comparable anymore with the skin temperature measured by the satellite. Most likely for this reason, both simulations differ from observations in the Norwegian Trench by higher SST values of about 4 K. While the thin skin layer can be cooled down very quickly, the ocean surface layer in the ROMS simulation may have a thickness of about 3 m in a 300 m deep area for instance and therefore cannot be cooled down in the same way.

Although modeled and observed sea surface heights show a reasonable agreement, some deviations can be found in particular during extreme events. A reason for this mismatch could be the ocean forcing at the open boundaries. ROMS is forced at the open boundaries by daily HYCOM mean surface elevation data which are not capable to represent storm surges coming from the Atlantic. Approaching low pressure systems cross the entire North Sea within 1 - 2 days, as shown, for instance, in the case of storm Uriah. The daily HYCOM data therefore provide only a low pass filtered signal of the incoming surge. Thus, resulting SSH changes in the simulations can solely arise from effects in the model domain itself. For this reason, a difference between model results and observations is expected.

4.2 Inaccuracies in Φ calculation

To estimate the error in the calculation of the single Φ terms of Eq. 3, which is rigorously derived from the general oceanographic equations as explained before, a comparison of total Φ change and the sum of the single Φ terms is shown by the black and red lines in Fig. 11b and Fig. 12b. As both values, Φ and the single Φ terms, are calculated directly from the model output, they should theoretically be consistent and completely match each other. No other external error sources, as errors in the model setup itself for instance, are expected to arise in this comparison. Although the two lines show a general good agreement, they do not completely match each other but show slight differences. These remaining deviations could arise from numerical inaccuracies and applied interpolations and probably could be decreased due to a higher temporal and spatial model resolution (to minimize the approximation errors

when going from the analytical to the numerical solution) or by the use of a term calculation which is closer to the applied model numerics.

4.3 Φ time series

4.3.1 Main Φ term - The vertical mixing response

The key factor dominating the destratification process during the storm event is the vertical mixing (term E). A comparison of the vertical mixing at both stations indicates the major difference in response to the storm: While at HPC two vertical mixing signals develop, only one signal occurs at Oysterground. In Fig. 13 the coupled and the two uncoupled simulation at HPC are compared. In contrast to the coupled run, the ERA-uncoupled run also only shows one vertical mixing peak, although this peak is stronger by reaching maximum Φ changing rates of about -7.5 Wm^{-3} instead of about -6 Wm^{-3} in the coupled simulation. This leads to a weaker erosion of the thermocline and thus to a shallower new SML. Due to this weaker vertical mixing, temperatures in the new mixed layer stay too high. This finally results in a temperature overestimation in the ERA-uncoupled simulation as shown in Sec. 3.3.4 at the SST minima created by the storm. In the WRF-uncoupled simulation an opposite situation occurs. Here also two signals occur, while the second one even leads to stratification. The first signal is much stronger due to the notably higher surface stress (Fig. 15c) directly at that point of time caused by the missing SST feedback in the coupling. Similar behavior of increased surface stresses during extreme events by neglecting the ocean SST feedback are mentioned by Small et al (2012). The authors found that SST cooling during the event leads to a significant reduction of surface momentum. This could be a result of less energy provided from the ocean to the atmosphere and thus to storm intensification due to higher temperatures at the ocean surface. The second vertical mixing signal shows a stabilizing effect since the water column is already complete mixed at that point of time due to the strong wind effect but other terms are additionally destratifying. As the vertical mixing continues it balances these other effects and thus shows a positive signal in $\delta_t \Phi$.

Summarized, two major interesting characteristics, regarding the occurrence of the vertical mixing signals, can be seen: Firstly, in the coupled simulation, station HPC area shows a different response of the vertical mixing than station Oysterground (namely two signals instead of one signal). Secondly, even at the same station (HPC area) a different behavior of the vertical mixing can be found between the coupled (produces two signals) and the ERA-uncoupled (produces one signal) simulation.

To investigate the different acting mechanisms, the interaction of tidal currents and wind stress is investigated closer (Fig. 15). The comparison of this figure and the temporal development of the vertical mixing shown before (Fig. 11c and Fig 12c) indicates the following: A strong vertical mixing only develops when strong wind stress and maximum flood currents occur simultaneously.

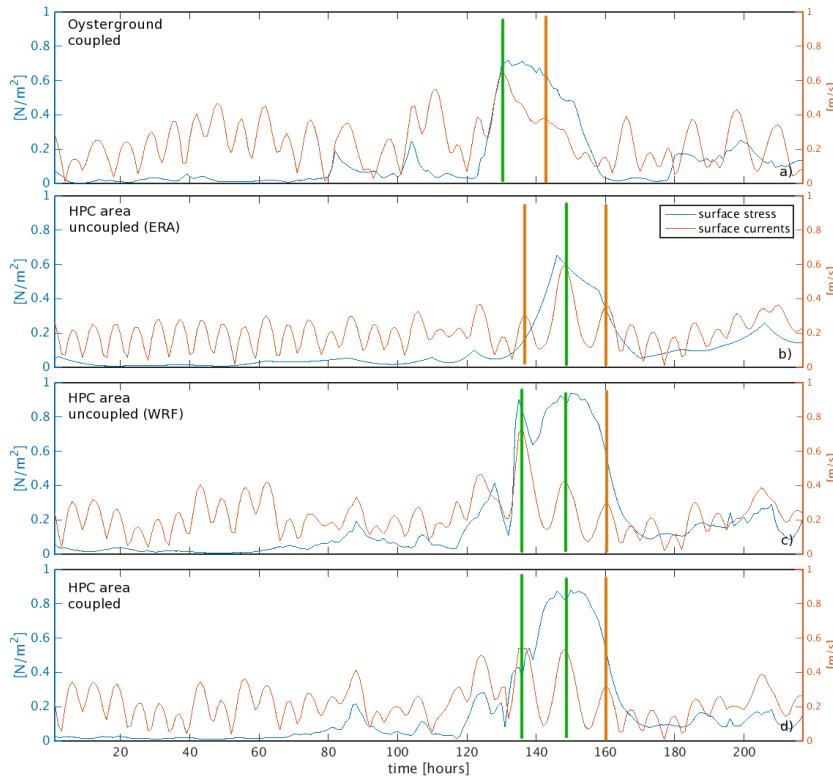


Fig. 15 Time series of surface currents (red line) and surfaces stresses (blue line) at Oysterground (a) and HPC area ERA-uncoupled (b), WRF-uncoupled (c) and coupled (d); vertical lines mark main vertical mixing time (green lines; see peak in the vertical mixing signal in Fig. 11c and Fig. 12c) or time when vertical mixing is expected due to maximum flood currents but is absent (orange lines; given by maxima of surface currents during storm event)

This is the case only once at Oysterground (around hour 131), when maximum tidal inflow and a surface stress of about 0.71 N/m^3 are reached (see Fig. 15a, green line). At the next incoming flood, around hour 143, the wind stress already decreased to about 0.63 N/m^3 , surface currents are weaker and no second strong vertical mixing arises anymore.

The situation is different at HPC area. Since this area is located upstream of the storm track (Fig. 1), the phase between high wind-speeds and the local flood is different. Both, the incoming flood at hour 136 as well as the flood at hour 148 lead to a very strong mixing (see Fig. 15d, green lines). The flood at hour 148 goes together with a strong surface stress of about 0.85 N/m^3 , and thus an expected mixing signal. Surprisingly, also the first incoming tidal current (at hour 136, first green line) creates a mixing signal, although the wind stress is even weaker compared to Oysterground (orange line) with about 0.55 N/m^3 where there is no mixing. The reason why mixing is still possible in

this case at HPC but not at Oysterground (even with these slightly stronger winds) is the different mixed layer depths at the respective point of time:

At Oysterground the first signal (hour 131 when maximum flood currents are reached) is directly produced in combination with a very strong wind. With its maximum intensity the storm is able to directly mix the water column up to about 23 m depth instantaneously with the first flood current (compare Fig. 11a, temperature development). Thus, for a potential mixing during the second flood, energy would be needed to mix the water column up to this depth and a relatively thick layer has to be moved.

In contrast, the weaker winds at HPC area act on a shallower SML during the first flood (hour 136). Due to the presence of this shallower SML, the weaker wind is able to produce a considerable mixing signal. This vertical mixing, however, only mixes the water column up to 17 m (compare Fig. 12a, temperature development) due to less energy. During the second flood at HPC area (hour 148), the maximum wind stress, which occurs at this point of time, hits an already weakened thermocline and is able to mix up to this not too deep SML depth. As a result, a second vertical mixing signal can be found.

Oey et al (2006) and Sun et al (2015) mathematically derive the required surface stress energy to mix a given ocean layer with a certain thickness over a certain density gradient (Eq. 2 of Oey et al, 2006 and Eq. 9 of Sun et al, 2015). Assuming a similar vertical density difference between the mixed surface and the deeper layer (as approximately given in the two cases: Oysterground at hour 143 and HPC area at hour 148), a mixing of the upper part of the water column with a surface layer of 22 m (Oysterground) would need about 30% more energy as a mixing of the upper water column with a surface layer of only 17 m (HPC area). In contrast to this, the actual surface stresses show the opposite behavior: The actual stress at Oysterground (0.63 N/m^2) is 30% lower than at the stress HPC (0.85 N/m^2).

The ERA-uncoupled simulation at HPC area also indicates only one vertical mixing signal. Fig. 15b illustrates that surface stresses during the first incoming maximum flood current (hour 136) are much too weak to produce a strong vertical mixing. This is an artifact of both: too low spatial (leads to less intensity) as well as temporal (leads to smoothing) resolution of the ERA-interim forcing data. This development of only one vertical mixing signal in the ERA-uncoupled simulation in combination with a likewise smoothed and less intense depth-mean straining term (which is the second strongest term at HPC, also supporting the destratification during the storm as explained below) leads to a remaining stratification in the ERA-uncoupled simulation at HPC. Thus, in the ERA-uncoupled simulation a new SML with a depth of about 17 m develops, whereas in the coupled simulation almost the entire water column gets mixed by the storm (up to the bottom at 32 m) with remaining Φ values of close to zero (Fig. 12a). The WRF-uncoupled simulations mixed the water column even stronger so that directly after the event no stratification at all remains.

Similar findings are summarized by Groeger et al (2015). The weaker winds in their coupled simulation lead to weaker vertical mixing.

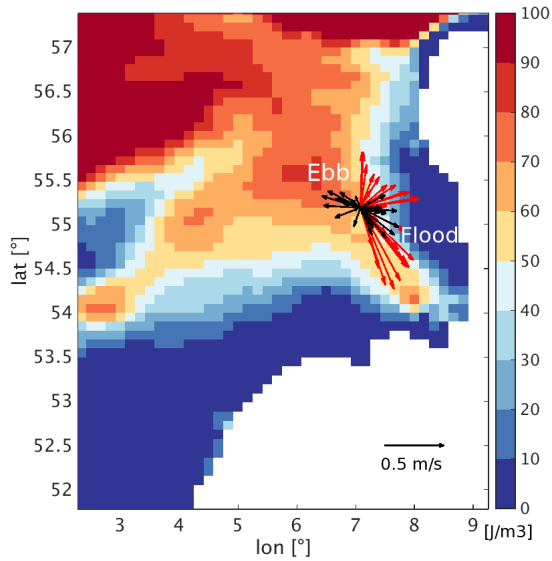


Fig. 16 Stratification (Φ) and flood/ebb surface currents at HPC area during standard conditions prior to the storm (black arrows with labeled standard direction of ebb and flood) and during storm Uriah (red arrows); multiple arrows refer to time steps over tidal cycle

4.3.2 Secondary Φ terms

Two dominating frequencies can be found in the different terms, an approximately 12-hourly and an approximately 24-hourly oscillation. The 12-hourly oscillation can be found in the horizontal advection (term A) and the depth-mean straining (term B) for instance, counteracting each other. This semidiurnal pattern is driven by the currents resulting from the M2 tide. At location HPC (compare Fig. 9c for location and Fig. 12 for temporal development), the counterclockwise general ocean circulation of the North Sea is superimposed by the strong tidal current in south-east (north-west) direction when flood (ebb) is developing. Fig. 16 illustrates the direction of currents and thus the tidal cycle during standard conditions prior to the storm (in black) and the modified situation during storm Uriah (in red). The simulation results indicate a destratification influence by horizontal Φ advection (negative term A) and simultaneously a stratification influence due to depth-mean straining (positive term B) when ebb develops and thus current directions are north-westward. In general, horizontal Φ advection leads to an increase (decrease) of stratification when stronger (weaker) stratified water is advected into the region of interest. As shown by the Φ pattern in Fig. 16, the water column south-eastwards from HPC area shows less stratification as the water column north-westwards. Thus, with every ebb (flood) flow, weaker (stronger) stratified water is advected by the tidal current to HPC area leading to the destratification (stratification) influence shown in the model simulation.

The situation is different for the depth-mean straining. Basically, this term mainly results from the vertical velocity gradient developing in the tidal flow. At the bottom, velocities are smaller due to bottom drag compared to surface velocities. Thus, a vertical velocity gradient develops, which leads to a stronger surface transport of water having certain properties and less transport of this water at the bottom. If the flow direction is coming from a lower density area going to a higher density area, the light water is transported faster and thus further at the surface compared to the bottom, leading to a stable stratification at locations in flow direction. As density is a function of temperature and salinity, lower density water develops, for instance, in low salinity areas as existing at the North Sea coastlines due to strong freshwater inflow by rivers. Thus, during ebb this lighter water is transported stronger at the surface from the south-east leading to a stratification in the HPC area (a positive term B during ebb). During flood the situation reverses and destratification occurs. This process is also known from several estuarine studies as Strain Induced Periodic Straining (SIPS) (see Simpson et al (1990), Sharples and Simpson (1993) or Souza and Simpson (1997)).

Differences between the coupled and uncoupled simulations can be found in these terms during the event while only small differences occur under standard conditions. As shown in Fig. 13a, strong differences occur in the horizontal advection. The surface stresses at hour 136 are much stronger in the WRF-uncoupled simulation pushing the depth-mean current strongest and farthest to the south-east, transporting water from regions with higher Φ values to areas with lower values and thus increasing stratification. This results in the strong peak reaching about $2 \times 10^{-4} W/m^3$. Surface stresses in the ERA-uncoupled simulation at that time are weakest and only turn slowly and with less intensity from the intensified southerly wind between hour 120 and 130 to the intense north-westerly wind of the event. As a result, depth-mean currents cannot adapt in the same rapidity as in the WRF-uncoupled simulation. Thus, depth-mean currents at hour 136 in the ERA-uncoupled simulation are oriented more to the north and thus are not directed to the maximum Φ gradient which results in a smaller signal in the horizontal advection at that time. The coupled simulation, again, behaves in between.

Furthermore, horizontal advection in the WRF-uncoupled simulation vanishes from hour 155 onwards. This is a result of the strongly intensified vertical mixing which results in a complete mixing of each water column in the entire region. Thus, independent of the currents, Φ values are zero and horizontal advection cannot occur anymore. But although each water column is completely mixed and Φ values become zero, a horizontal gradient of depth-mean density still occurs, as horizontal mixing does not have a notable influence (Fig. 12c or d). For that reason, even in the WRF-uncoupled simulation a tidal signal in the depth-mean straining (Fig. 13b) can still be observed. Also the differences between the simulations in the depth-mean straining around hour 130 originate from the much weaker surface stresses in the ERA-uncoupled simulation. Only the ERA-uncoupled simulation shows a stabilizing effect of depth-mean straining while the other two simulations show destratification at

that time. These weaker surface stresses in the ERA-uncoupled simulation allow the surface currents to be directed to the north-west, which moves lighter water from the coast on top of the denser water in the north-west, the much stronger surface stresses in the WRF-uncoupled simulation and in the coupled simulation push the surface currents already to the north-east and thus move denser water on top of lighter water leading to destratification.

The mentioned 24-hourly pattern of the surface fluxes as well as inner sources (term F and G) are driven by incoming solar radiation. During day, the incoming solar radiation heats up the ocean surface and produces warmer and lighter water at the surface and thus increases stratification. Furthermore, solar radiation penetrating into the water column heats the water in deeper layers in a similar way, also leading to stratification. During the storm event a stronger heat loss to the atmosphere can be observed, which is unusual during this time of the year. This heat loss is assumed to be forced by a combination of less heat gain, for instance due to clouds that lead to less incoming shortwave radiation, as well as more heat loss, for instance due to a decrease in atmospheric surface temperatures during the event. This heat loss, however, is not the main factor responsible for the strong SST cooling during the storm (compare the relative amount of term F and G in Fig. 11 and Fig. 12).

4.4 Φ spatial analysis

The overview of the development of stratification as shown in Fig. 9 clearly indicates a stronger destratification process at the eastern coast of the North Sea. Following the detailed time series analysis of Sec. 4.3 this stronger destratification is mainly caused by a different temporal interaction of incoming flood currents and passing wind stresses, an interaction which defines the vertical mixing. The physical processes dominating the stratification and destratification in the entire North Sea during normal conditions (prior to the storm event) as illustrated in Fig. 10a can be explained as follows. Near the coastlines, in particular in the eastern part of the North Sea, the salinity structure is strongly formed by riverine freshwater discharge. This freshwater and the resulting strong salinity gradient combined with the temperature gradient lead to a strong density gradient near the coast, in particular in the eastern North Sea. As a result of this horizontal gradient, the depth-mean straining (term B, dark blue) is the dominant process in this region. The vertical mixing (term E, rose) dominates in regions which show strong tides and shallow waters. In deeper waters, a higher Φ value is present. Hofmeister et al (2009) mention the connection between stratification strength and several physical processes: In areas of strong stratification, they state, vertical (term D, dark green) and horizontal (term A, light blue) advection are supported. A similar behavior can be found in the present results: The area between about -1° and 2° longitude and 55° and 57° latitude is dominated by these two terms and even during the storm event vertical mixing cannot overrule this signal (Fig. 10a and b).

The structure of these two terms that mainly influence this area corresponds very well, as Hofmeister et al (2009) explain, to a similar structure in a very high stratification and thus high Φ values (see Fig. 9 at the same location, in particular the two rounded patterns near coast defined by the $100 J/m^3$ contour line).

Surface fluxes (Fig. 10a, term F, red) are generally uniformly distributed over the entire North Sea but only in the central part they are not overlaid by other processes.

During the storm event the situation is different and destratification in almost the entire North Sea is dominated by vertical mixing, except for a few very deep areas or areas which are in addition located further away from the storm track.

4.5 Potential relevance for the ecosystem

From the results of this study it can be expected that the loss of stratification and the involved mixing during summer storm Uriah in 2007 had an important influence on the local ecosystem. Carlotti and Radach (1996) discuss the impact of summer storms on marine biology. In their study, which is based on a population dynamics model, the reformation of the thermocline led to a favorable growth situation for phytoplankton (and thus zooplankton). The bloom was triggered by the excess nutrients released from the former bottom waters, which were sheltered by the thermocline.

Fig. 17 shows the maximum restratification reached after the storm event. Φ values are calculated until mid September, which corresponds approximately to day 250 in Fig. 8. As SST are already decreasing at this time due to the usual seasonal cycle, after this point of time during autumn and winter, further restratification will not occur anymore. Thus the percentage of restratification can be understood as maximum restratification for the rest of the year 2007. Results are presented as percentage of the local pre-storm stratification. The analysis is limited to strongly influenced regions with a loss of stratification larger than $20 J/m^3$ during the storm. The results indicate that only limited stratification could reestablish afterwards. This could have a notable impact on the local ecosystem. Measurements to define the depth of the euphotic zone in that region Aarup (2002) show, by a Secchi depth of about 6-8 m, that the zone where there is still enough sunlight available for phytoplankton to grow ends in about 12-16 m depth. Following the results of the present study, the application of high resolution atmospheric data and interactive coupling lead to large differences for the ecosystem compared to a 3-hourly standard forcing: Whereas the coupled simulation resulted in a almost completely mixed water column at Oysterground (32 m depth), the ERA-uncoupled simulation only reaches a vertical mixing of up to 17 m. The WRF-uncoupled simulation shows an about 4-times stronger vertical mixing with $\delta_t\Phi$ values of about $20W/m^3$ due to twice that strong surface stresses of about $9 N/m^2$. This leads to an immediate complete mixing. In the ERA-uncoupled simulation the newly de-

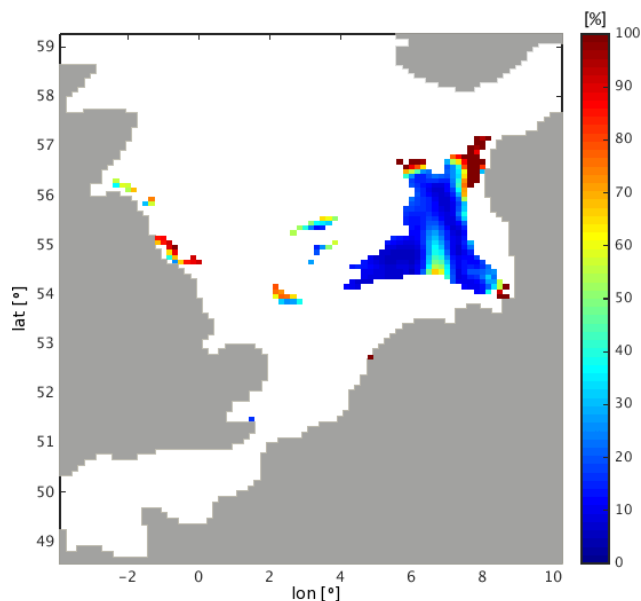


Fig. 17 Maximum restratification during 2007 after summer storm Uriah in percent of original stratification before. Values are only considered for areas with a considerable change of stratification of more than $20 \frac{J}{m^3}$ during storm (compare Fig. 9c, orange and red areas)

veloped SML mainly stays inside of the euphotic zone, as defined by Aarup (2002). This offers favorable growth conditions for phytoplankton by providing nutrients from formerly sheltered deeper layers. In addition, the thickness of the new SML still provides enough sunlight to grow, as the thermocline is still above the euphotic depth. In combination, a bloom could be enforced. In the situation of a stronger mixing, as seen in the coupled simulation (Fig. 12), the excess levels of nutrients would be higher than in the ERA-uncoupled situation. However, since the newly formed SML extends over the euphotic depth, the triggering of a bloom could be prevented. The reason is that due to the thicker SML phytoplankton could stay for longer time in light limited water depths. A similar reasoning can be found by Skogen et al (2011) who investigated the impact of high wind speeds and thus a thickening of the SML onto primary production. A further side effect of stronger vertical mixing and thus a fully mixed water column is that benthic sediments can easily be distributed over the entire water column. This would result in notable differences between the simulations, in particular regarding the strongly intensified vertical mixing in the WRF-uncoupled simulation. This would result in an enlarged sediment mobilization and thus a reduction of the euphotic depth and therefore a stronger light attenuation.

5 Summary and outlook

A coupled regional ocean-atmosphere system has been used to simulate a strong summer storm event in the North Sea region. The response in SST is well captured compared with observations. To investigate changes in the stratification, a detailed analysis of the changes in the Potential Energy Anomaly (Φ) following Burchard and Hofmeister (2008) is performed. The individual terms leading to changes in Φ are computed and compared. The vertical mixing is the major process responsible for the destratification during this storm event. This is in contrast to the initial assumption that the drop in SST was mainly caused by advection, straining or heat loss to the atmosphere. The analysis further revealed that interaction and phase differences between flood currents and surface stresses have a strong impact on the resulting vertical mixing. A comparison between a coupled, a classical ERA-uncoupled simulation with lower-resolution forcing and a WRF-uncoupled simulation which provides a high-resolution forcing, during this summer storm indicates an SST overestimation of the ERA-uncoupled simulation during this event as well as a SST underestimation in the WRF-uncoupled simulation in particular prior to the event. This is mainly caused by an under- and overestimation of the vertical mixing. A detailed analysis of the physical processes suggests that the SST overestimation most likely results from a too low spatial and/or temporal resolution of the atmospheric forcing data, in particular the wind fields, for the simulation of an extreme event. The SST underestimation results of the neglect of an SST feedback during the event.

The illustrated differences between the coupled and the two uncoupled simulations suggest a crucial influence on the ecosystem: After the storm, the new depth of the thermocline is either located inside (ERA-uncoupled) or even outside (coupled, WRF-uncoupled) the euphotic zone, which might have a crucial impact on the triggering of phytoplankton blooms as well as on sediment mobilization. This leads to the suggestion that, during extreme events, an appropriately high temporal and spatial resolution of the forcing, a good representation of the tides as well as a high-resolution SST feedback is necessary in particular for ecosystem modeling but also for sediment modeling. This suggestion is supposed to be also valid for other tidally influenced regions.

Acknowledgements We would like to thank the International Research Training Group INTERCOAST and the Deutsche Forschungsgemeinschaft (DFG) for funding for this study. Atmospheric surface data for evaluation were kindly provided by the German Deutsche Wetterdienst (DWD) and the National Center for Environmental Predictions (NCEP).

We acknowledge the public deployment of very valuable information and different tools for pre- and post-processing of ROMS and WRF data by the ROMS/TOMS Group, ROMS AGRIF (ROMSTOOLS), Emanuele Di Lorenzo (ROMS Numerical Toolbox), Hernan G. Arango, John C. Warner and the COAWST team and MMM/NCAR.

Many thanks to Mark Hadfield and colleagues for support and fruitful discussions and also for the possibility to visit and work at NIWA Wellington during a part of this study.

Further thanks for valuable general discussions regarding the COAWST system, the PEA analysis and North Sea modeling are going to A. Aretxabaleta, H. Burchard, T. Pohlmann

and colleagues and J. C. Warner and colleagues.

We also would like to thank the two anonymous reviewers, who clearly helped with their very constructive, detailed and careful comments to improve this work.

References

- Aarup T (2002) Transparency of the North Sea and Baltic Sea, a Secchi Depth data mining study. *Oceanologia* 44(3):323–337
- Berg P, Wagner S, Kunstmann H, Schaedler G (2013) High resolution regional climate model simulations for Germany: part I validation. *Climate Dynamics* 40(1-2):401–414, DOI 10.1007/s00382-012-1508-8, URL <http://dx.doi.org/10.1007/s00382-012-1508-8>
- Booij N, Ris RC, Holthuijsen LH (1999) A third-generation wave model for coastal regions: 1. Model description and validation. *Journal of Geophysical Research: Oceans* 104(C4):7649–7666, DOI 10.1029/98JC02622, URL <http://dx.doi.org/10.1029/98JC02622>
- Burchard H, Hofmeister R (2008) A dynamic equation for the potential energy anomaly for analysing mixing and stratification in estuaries and coastal seas. *Estuarine, Coastal and Shelf Science* 77(4):679–687, DOI <http://dx.doi.org/10.1016/j.ecss.2007.10.025>, URL <http://www.sciencedirect.com/science/article/pii/S0272771407004945>
- Carlotti F, Radach G (1996) Seasonal dynamics of phytoplankton and *Calanus finmarchicus* in the North Sea as revealed by a coupled one-dimensional model. *Limnology and Oceanography* 41(3):522–539, DOI 10.4319/lo.1996.41.3.0522, URL <http://dx.doi.org/10.4319/lo.1996.41.3.0522>
- Chassignet EP, Hurlburt HE, Smedstad OM, Halliwell GR, Hogan PJ, Wallcraft AJ, Baraille R, Bleck R (2007) The HYCOM (HYbrid Coordinate Ocean Model) data assimilative system. *Journal of Marine Systems* 65(1-4):60–83, DOI <http://dx.doi.org/10.1016/j.jmarsys.2005.09.016>, URL <http://www.sciencedirect.com/science/article/pii/S0924796306002855>, marine Environmental Monitoring and Prediction Selected papers from the 36th International Liege Colloquium on Ocean Dynamics 36th International Liege Colloquium on Ocean Dynamics
- Delhez E, Damm P, de Goede E, de Kok J, Dumas F, Gerritsen H, Jones J, Ozer J, Pohlmann T, Rasch P, Skogen M, Proctor R (2004) Variability of shelf-seas hydrodynamic models: lessons from the NOMADS2 Project. *Journal of Marine Systems* 45(1-2):39–53, DOI <http://dx.doi.org/10.1016/j.jmarsys.2003.09.003>, URL <http://www.sciencedirect.com/science/article/pii/S0924796303001313>
- ECMWF (August 2016) Era-interim. <http://www.ecmwf.int/en/research/climate-reanalysis/era-interim>, URL <http://www.ecmwf.int/en/research/climate-reanalysis/era-interim>
- Egbert GD, Erofeeva SY (2002) Efficient inverse modeling of barotropic ocean tides. *Journal of Atmospheric and Oceanic Technology* 19:183–204

- Egbert GD, Bennett AF, Foreman MGG (1994) TOPEX/POSEIDON tides estimated using a global inverse model. *Journal of Geophysical Research: Oceans* 99(C12):24,821–24,852, DOI 10.1029/94JC01894, URL <http://dx.doi.org/10.1029/94JC01894>
- Gräwe U, Holtermann P, Klingbeil K, Burchard H (2015) Advantages of vertically adaptive coordinates in numerical models of stratified shelf seas. *Ocean Modelling* 92:56–68, DOI <http://dx.doi.org/10.1016/j.ocemod.2015.05.008>, URL <http://www.sciencedirect.com/science/article/pii/S1463500315000979>
- Groeger M, Dieterich C, Meier M, Schimanke S (2015) Thermal air-sea coupling in hindcast simulations for the North Sea and Baltic Sea on the NW European shelf. *Tellus A* 67, URL <http://www.tellusa.net/index.php/tellusa/article/view/26911>
- Haidvogel D, Arango H, Budgell W, Cornuelle B, Curchitser E, Lorenzo ED, Fennel K, Geyer W, Hermann A, Lanerolle L, Levin J, McWilliams J, Miller A, Moore A, Powell T, Shchepetkin A, Sherwood C, Signell R, Warner J, Wilkin J (2008) Ocean forecasting in terrain-following coordinates: Formulation and skill assessment of the Regional Ocean Modeling System. *Journal of Computational Physics* 227(7):3595–3624, DOI <http://dx.doi.org/10.1016/j.jcp.2007.06.016>, URL <http://www.sciencedirect.com/science/article/pii/S0021999107002549>
- Haney RL (1991) On the Pressure Gradient Force over Steep Topography in Sigma Coordinate Ocean Models. *Journal of Physical Oceanography* 21:610–619
- Hofmeister R, Burchard H, Bolding K (2009) A three-dimensional model study on processes of stratification and destratification in the Limfjord. *Continental Shelf Research* 29:1515–1524, DOI 10.1016/j.csr.2009.04.004
- Holt J, Umlauf L (2008) Modelling the tidal mixing fronts and seasonal stratification of the Northwest European Continental shelf. *Continental Shelf Research* 28(7):887–903, DOI <http://dx.doi.org/10.1016/j.csr.2008.01.012>, URL <http://www.sciencedirect.com/science/article/pii/S0278434308000241>
- Holt JT, James ID (1999) A simulation of the Southern North Sea in comparison with measurements from the North Sea Project. Part 1: Temperature. *Continental Shelf Research* 19(8):1087–1112, DOI [http://dx.doi.org/10.1016/S0278-4343\(99\)00015-1](http://dx.doi.org/10.1016/S0278-4343(99)00015-1), URL <http://www.sciencedirect.com/science/article/pii/S0278434399000151>
- Jacob R, Larson J, Ong E (2005) M x N Communication and Parallel Interpolation in CCSM3 Using the Model Coupling Toolkit. *International Journal for High Performance Computing Applications* 19:293–307
- Larson J, Jacob R, Ong E (2005) The model coupling toolkit: A new Fortran90 toolkit for building multiphysics parallel coupled models. *International Journal of High Performance Computing Applications* 19:277–292
- van Leeuwen S, Tett P, Mills D, van der Molen J (2015) Stratified and nonstratified areas in the North Sea: Long-term variability and biological and policy implications. *Journal of Geophysical*

- Research: *Oceans* 120(7):4670–4686, DOI 10.1002/2014JC010485, URL <http://dx.doi.org/10.1002/2014JC010485>
- Lenhart HJ, Pohlmann T (2004) North Sea hydrodynamic modelling: a review. *Senckenbergiana maritima* 34(1-2):53–88, DOI 10.1007/BF03043229, URL <http://dx.doi.org/10.1007/BF03043229>
- Loewe P, Klein H, Weigelt-Krenz S (2013) System Nordsee : Zustand und Entwicklungen. Berichte des BSH. Tech. rep., Bundesamt für Seeschifffahrt und Hydrographie, Hamburg and Rostock
- Mathis M, Mayer B, Pohlmann T (2013) An uncoupled dynamical down-scaling for the North Sea: Method and evaluation. *Ocean Modelling* 72:153–166, DOI <http://dx.doi.org/10.1016/j.ocemod.2013.09.004>, URL <http://www.sciencedirect.com/science/article/pii/S1463500313001662>
- Oey LY, Ezer T, Wang DP, Fan SJ, Yin XQ (2006) Loop Current warming by Hurricane Wilma. *Geophysical Research Letters* 33(8):1–4, DOI 10.1029/2006GL025873, URL <http://dx.doi.org/10.1029/2006GL025873>
- Penven P, Marchesiello P, Debreu L, Lefevre J (2007) Software tools for pre- and post-processing of oceanic regional simulations. *Environmental Modelling and Software* 23:660–662
- Perrie W, Ren X, Zhang W, Long Z (2004) Simulation of extratropical Hurricane Gustav using a coupled atmosphere-ocean-sea spray model. *Geophysical Research Letters* 31(3):1–4, DOI 10.1029/2003GL018571, URL <http://dx.doi.org/10.1029/2003GL018571>
- Pohlmann T (1996) Calculating the development of the thermal vertical stratification in the North Sea with a three-dimensional baroclinic circulation model. *Continental Shelf Research* 16(2):163–194, DOI [http://dx.doi.org/10.1016/0278-4343\(95\)00018-V](http://dx.doi.org/10.1016/0278-4343(95)00018-V), URL <http://www.sciencedirect.com/science/article/pii/027843439500018V>
- Pullen J, Doyle JD, Haack T, Dorman C, Signell RP, Lee CM (2007) Bora event variability and the role of air-sea feedback. *Journal of Geophysical Research-Oceans* 112(C3):1–17, DOI 10.1029/2006jc003726, URL <http://www.wiley.com/go/doi/10.1029/2006jc003726>, URL <http://www.wiley.com/go/doi/10.1029/2006jc003726>
- Purkiani K, Becherer J, Floeser G, Gräwe U, Mohrholz V, Schuttelaars HM, Burchard H (2015) Numerical analysis of stratification and destratification processes in a tidally energetic inlet with an ebb tidal delta. *Journal of Geophysical Research: Oceans* 120(1):225–243, DOI 10.1002/2014JC010325, URL <http://dx.doi.org/10.1002/2014JC010325>
- Reynolds RW, Smith TM, Liu C, Chelton DB, Casey KS, Schlax MG (2007) Daily High-Resolution-Blended Analyses for Sea Surface Temperature. *Journal of Climate* 20:5473–5496
- Schrum C, Hbner U, Jacob D, Podzun R (2003) A coupled atmosphere - ice - ocean model for the North Sea and the Baltic Sea. *Climate Dynamics* 21(2):131–151, DOI 10.1007/s00382-003-0322-8, URL <http://dx.doi.org/10.1007/s00382-003-0322-8>
- Schrum C, Alekseeva I, John MS (2006) Development of a coupled physical - biological ecosystem model ECOSMO: Part I: Model description and validation for the North Sea. *Journal of Marine Systems*

- 61(1-2):79–99, DOI <http://dx.doi.org/10.1016/j.jmarsys.2006.01.005>, URL <http://www.sciencedirect.com/science/article/pii/S0924796306000297>
- Sharples J, Simpson J (1993) Periodic frontogenesis in a region of freshwater influence. *Estuaries* 16(1):74–82, DOI 10.2307/1352765, URL <http://dx.doi.org/10.2307/1352765>
- Shchepetkin AF, McWilliams JC (2005) The regional oceanic modeling system (ROMS): a split-explicit, free-surface, topography-following-coordinate oceanic model. *Ocean Modelling* 9(4):347–404, DOI <http://dx.doi.org/10.1016/j.ocemod.2004.08.002>, URL <http://www.sciencedirect.com/science/article/pii/S1463500304000484>
- Simpson J (1971) Density stratification and microstructure in the western Irish sea. *Deep Sea Research and Oceanographic Abstracts* 18(3):309–319, DOI [http://dx.doi.org/10.1016/0011-7471\(71\)90036-2](http://dx.doi.org/10.1016/0011-7471(71)90036-2), URL <http://www.sciencedirect.com/science/article/pii/0011747171900362>
- Simpson J, Bowers D (1981) Models of stratification and frontal movement in shelf seas. *Deep Sea Research Part A Oceanographic Research Papers* 28(7):727–738, DOI [http://dx.doi.org/10.1016/0198-0149\(81\)90132-1](http://dx.doi.org/10.1016/0198-0149(81)90132-1), URL <http://www.sciencedirect.com/science/article/pii/0198014981901321>
- Simpson J, Crisp DJ, Hearn C (1981) The Shelf-Sea Fronts: Implications of their Existence and Behaviour [and Discussion]. *Philosophical Transactions of the Royal Society of London A: Mathematical, Physical and Engineering Sciences* 302(1472):531–546, DOI 10.1098/rsta.1981.0181
- Simpson J, Brown J, Matthews J, Allen G (1990) Tidal straining, density currents, and stirring in the control of estuarine stratification. *Estuaries* 13(2):125–132, DOI 10.2307/1351581, URL <http://dx.doi.org/10.2307/1351581>
- Simpson JH, Hunter JR (1974) Fronts in the Irish Sea. *Nature* 250:404–406
- Skamarock WC, Klemp JB, Dudhia J, Gill DO, Barker DM, Duda MG, Huang X, Wang W, Powers JG (2008) A Description of the Advanced Research WRF Version 3. Tech. rep., 459, NCAR, Boulder, Colorado, USA
- Skogen MD, Drinkwater K, Hjllo SS, Schrum C (2011) North Sea sensitivity to atmospheric forcing. *Journal of Marine Systems* 85(3-4):106–114, DOI <http://dx.doi.org/10.1016/j.jmarsys.2010.12.008>, URL <http://www.sciencedirect.com/science/article/pii/S0924796310002241>
- Small RJ, Carniel S, Campbell T, Teixeira J, Allard R (2012) The response of the Ligurian and Tyrrhenian Seas to a summer Mistral event: A coupled atmosphere-ocean approach. *Ocean modelling* 48:30–44
- Souza AJ, Simpson JH (1997) Controls on stratification in the Rhine ROFI system. *Journal of Marine Systems* 12(1-4):311–323, DOI [http://dx.doi.org/10.1016/S0924-7963\(96\)00105-4](http://dx.doi.org/10.1016/S0924-7963(96)00105-4), URL <http://www.sciencedirect.com/science/article/pii/S0924796396001054>
- Sun J, Oey LY, Chang R, Xu F, Huang SM (2015) Ocean response to typhoon Nuri (2008) in western Pacific and South China Sea. *Ocean Dynamics* 65(5):735–749, DOI 10.1007/s10236-015-0823-0, URL <http://dx.doi.org/10.1007/s10236-015-0823-0>

- Warner JC, Sherwood CR, Arango HG, Signell RP (2005) Performance of four turbulence closure models implemented using a generic length scale method. *Ocean Modelling* 8(1-2):81–113, DOI <http://dx.doi.org/10.1016/j.ocemod.2003.12.003>, URL <http://www.sciencedirect.com/science/article/pii/S1463500303000702>
- Warner JC, Sherwood CR, Signell RP, Harris CK, Arango HG (2008) Development of a three-dimensional, regional, coupled wave, current, and sediment-transport model. *Computers & Geosciences* 34(10):1284–1306, DOI <http://dx.doi.org/10.1016/j.cageo.2008.02.012>, URL <http://www.sciencedirect.com/science/article/pii/S0098300408000563>
- Warner JC, Armstrong B, He R, Zambon JB (2010) Development of a Coupled Ocean - Atmosphere - Wave - Sediment Transport (COAWST) Modeling System. *Ocean Modelling* 35(3):230–244, DOI <http://dx.doi.org/10.1016/j.ocemod.2010.07.010>, URL <http://www.sciencedirect.com/science/article/pii/S1463500310001113>